

AN INVESTIGATION OF HYDROGEN TRANSFER IN COPROCESSING USING MODELS AND REDUCED RESIDS

Shu-Li Wang and Christine W. Curtis
Chemical Engineering Department
Auburn University, AL 36849-5127

Abstract

Hydrogen donor reactions in the coprocessing of coal and petroleum resids have been investigated using different hydrogen-rich models and reduced resids as donors and aromatics as acceptors. Three hydrogen-rich donor species were compared: cyclic olefins, hydroaromatics, and cycloalkanes; the aromatic acceptors included pyrene and anthracene; and the resids were reduced by the Birch method. Hydrogen was transferred most readily at 380°C by cyclic olefins, followed by hydroaromatics, and the least was transferred by cycloalkanes. Catalysis by thiophenol promoted the hydrogen transfer by the cycloalkanes at 380°C but had little effect at 440°C. Reduced resids transferred substantially more hydrogen to an aromatic species than did the untreated resids. In a tertiary system of reduced resid, cycloalkane, and aromatic, the reduced resids yielded more hydrogen transfer and promoted hydrogen donation from the cycloalkanes in a nitrogen atmosphere. Reduction of resids by the Birch method appeared to be an effective means of increasing the hydrogen donor ability of resids.

Introduction

Hydrogen donor reactions are important in the transfer of hydrogen from hydrogen-rich compounds to aromatic species in the liquefaction of coal. Different hydrogen-rich compounds have different propensities for donating hydrogen under liquefaction conditions; just as different hydrogen acceptors have different propensities for accepting hydrogen. In this study, the ability of three different hydrogen donors to donate hydrogen and the efficiency of their hydrogen transfer to aromatic species were compared under both hydrogen and nitrogen atmospheres.

The compounds compared were cyclic olefins, which have been shown to release their hydrogen quickly under liquefaction conditions, hydroaromatics, that are typically present in coal liquids and are known hydrogen donors, and cycloalkanes, that are present in resids and do not readily donate their hydrogen. Promotion of hydrogen transfer from the hydrogen-rich cycloalkanes to aromatics is of special interest because these structures are prevalent in resids and offer an indigenous source of hydrogen. Rudnick [1986a,b] has shown that the introduction of an organic sulfur compound promotes this type of hydrogen transfer. In this work, catalytic reactions with organic sulfur were performed to evaluate the effect on the hydrogen transfer from cycloalkanes to aromatics at 380°C and 440°C under both nitrogen and hydrogen atmospheres. These results were compared to thermal reactions at the same conditions.

In the coprocessing of coal with resid, resids have limited ability to solvate coal and to donate hydrogen because of the predominance of indigenous saturated structures. Increasing the hydrogen donability of the chemical species of the resid should enhance the ability of the resid to solvate coal. This enhancement was induced by reducing resids by the Birch reduction method [Birch and Rao, 1972] which is known for producing cyclic olefinic structures from

aromatic species. The ability of these reduced resids to transfer hydrogen to aromatics was determined and compared to the parent resids.

Experimental

Materials and Analysis. Reactions were performed using the following hydrogen-rich compounds: cyclic olefins, isotetralin (ISO) which was synthesized in our laboratory, and hexahydroanthracene (HHA) from Aldrich; hydroaromatics, tetralin (TET) and 9,10-dihydroanthracene (DHA) both from Aldrich; and a cycloalkane, perhydropyrene (PHP) from Aldrich. The compounds used as hydrogen acceptors in these reactions were anthracene (ANT) and pyrene (PYR) both obtained from Aldrich. Thiophenol was used as a catalyst for promoting the transfer of hydrogen from cycloalkanes to aromatics. The catalyst was introduced at a level of 2,000 ppm of sulfur. The reaction products were analyzed by gas chromatography using a Varian 3300 gas chromatograph with FID detection and biphenyl as the internal standard. Qualitative analysis of the products was conducted with a VG70 EHF GC-mass spectrometer.

Thermal and catalytic reactions were performed with the parent resids and treated resids which had been reduced by the Birch method [Birch and Rao, 1972]. The Birch reduction method reduces aromatics in the resid to cyclic olefins and other partially saturated forms by adding Na, alcohol, and ammonia to the resid which is dissolved in tetrahydrofuran (THF) as the solvent. The resids that were used in these reactions were Maya obtained from Amoco Oil Co., a deasphalted resid from a deasphalting resid unit (DAU) from Exxon and south Louisiana resid (S. LA) also from Exxon; the hydrogen acceptor for the reactions was ANT; and the catalyst was 2000 ppm sulfur introduced at thiophenol. The products from these resid reactions were analyzed by gas chromatography to determine the reaction products from both the model donors and acceptors and by solvent fractionation to determine the products from the resid. The solvents used in the extraction of the thermal products were toluene (TOL) and THF, but in the catalytic reactions, hexane (HEX) was also used.

Reaction Procedures. Reactions were performed in 20 cm³ stainless steel tubular microreactors with single reactants charged at 0.1 g and with binary reactants charged at 0.1 g aromatic and the hydrogen-rich compound introduced at a 1:1 or 5:1 weight ratio to the aromatic. The reaction conditions for the thermal model reactions were 380°C, 30 minutes, nitrogen or hydrogen at 400 psi at ambient, and horizontal agitation at 435 rpm.

Definitions. The following definitions were used: Percent hydrogenation (% HYD) is defined as the moles of hydrogen required to achieve the liquid products as a percentage of the moles of hydrogen required to produce the most hydrogenated product. In the case of ANT, octahydroanthracene (OHA) was considered the most hydrogenated product; in the case of pyrene, the most hydrogenated product was taken to be hexahydropyrene (HHP). Hydrogen efficiency is defined as the moles of hydrogen accepted by the hydrogen acceptor divided by the moles of hydrogen released by the hydrogen donor. The amount of gaseous hydrogen that was accepted by the hydrogen donor is defined as the moles of hydrogen accepted by the hydrogen acceptor under a hydrogen atmosphere minus the moles of hydrogen accepted by the hydrogen acceptor under a nitrogen atmosphere.

Results and Discussion

Thermal Reactions of Hydrogen-Rich Compounds with Aromatics. Reactions of hydrogen-rich compounds, cyclic olefins, hydroaromatics and cycloalkanes, with aromatic species, ANT and PYR, were performed in N₂ and H₂ atmospheres. The purpose of these

experiments was to determine how much hydrogen was released from the hydrogen donor and how much of that hydrogen was accepted by the aromatic species. The reaction of the cyclic olefins with the aromatics resulted in the products of tetralin (TET), 1,2- and 1,4-dihydronaphthalene (DHN), and naphthalene (NAP) from ISO and of OHA, tetrahydroanthracene (THA), DHA and ANT from HHA. The hydroaromatics produced NAP from TET and THA plus ANT from DHA. The cycloalkane PHP only produced PYR as its product. The amount of hydrogen released from the hydrogen-rich compounds was in the order of cyclic olefins > hydroaromatics > cycloalkanes. The amount of hydrogen released from each species was dependent upon the type of atmosphere and acceptor present as well as upon the amount of hydrogen-rich compound present. These results are shown in Table 1.

ANT, as an acceptor, formed DHA and THA as products while PYR formed dihydro-pyrene (DHP), tetrahydropyrene (THP) and hexahydropyrene (HHP) as products. The % HYD of the aromatic species in individual reactions and in binary reactions with hydrogen-rich species is presented in Table 1. The most hydrogenation of the aromatic species occurred in the presence of the cyclic olefins and in a H₂ atmosphere. ANT was more reactive than PYR when reacted with the same hydrogen donor and at the same conditions.

The hydrogen efficiency of the systems was also compared in Table 1. As the value for hydrogen efficiency approached one, then the amount of hydrogen released was equal to the amount of hydrogen accepted. The hydrogen efficiency of the systems in the N₂ atmosphere showed that the cyclic olefins were the least efficient since they released substantially more hydrogen than the aromatic species was able to accept. In the H₂ atmosphere, hydrogen efficiencies of greater than one were obtained which indicated that gaseous hydrogen was participating in the reactions. The moles of gaseous H₂ incorporated into the reaction products from the hydrogen acceptor varied with the system as shown in Table 1.

Catalytic Reactions of Hydrogen-Rich Compounds with Aromatics. Catalytic reactions were performed with a reaction system of PHP with ANT at a weight ratio of PHP to ANT of 1:1 and 5:1 in both N₂ and H₂ atmospheres at reaction temperatures of 380 and 440°C. The catalyst was 2000 ppm of sulfur introduced as thiophenol. The products produced from PHP were HHP and PYR at both reaction temperatures; the products produced from ANT were DHA at 380°C and DHA, THA, and OHA at 440°C. The amount of hydrogen donated and accepted from these reactions was compared to that in the thermal reactions at the same conditions (Table 2).

The addition of the sulfur catalyst increased the amount of hydrogen donation from PHP. The catalyst also increased the amount of hydrogen acceptance and, hence, hydrogenation of ANT to DHA in both atmospheres. Under thermal conditions, PHP produced only PYR as the product while under catalytic conditions HHP was formed in larger amounts than PYR. The catalysis of hydrogen donation and acceptance by S was observed most in the PHP/ANT system at a 5:1 weight ratio at 380°C in H₂ and N₂ compared to the thermal reaction where a substantial increase in the hydrogenation of the aromatic was obtained compared to the thermal reaction. The promotion of the reaction by S was also observed in N₂ but not in H₂ at 440°C. The higher temperature of 440°C with H₂ as the atmosphere seemed to have more effect on hydrogen donation and acceptance than did the catalyst, because the % HYD's of ANT were equivalent in thermal and catalytic reactions.

The hydrogen efficiency in N₂ shown in Table 2 was always less than one with the hydrogen efficiency of 5:1 PHP to ANT reaction systems frequently having a higher efficiency than the 1:1 ratio. The hydrogen efficiencies for the reactions in the hydrogen atmosphere were always greater than one indicating incorporation of gaseous hydrogen into the reaction

products. The number of moles of gaseous hydrogen incorporated was substantially higher for the higher temperature reactions at 440°C than those at 380°C.

Hydrogen Transfer from Resids. The purpose of this work was to evaluate the efficacy of hydrogen transfer from hydrogen-enriched reduced resids to an aromatic species and to compare that to the hydrogen transfer from the parent resid. The systems used were the reduced and parent resids with the acceptor ANT and the ternary system of a reduced or parent resid with ANT and the hydrogen-rich species, PHP.

The reactions of the reduced and parent resids with ANT in both N₂ and H₂ atmospheres are presented in Table 3. All three of the reduced resids yielded substantially more hydrogenation of ANT to DHA and THA than did the parent resids. The hydrogen atmosphere promoted more hydrogenation of ANT than did nitrogen regardless of whether the resid was reduced or was the parent. The product distributions from each of the resid reactions are given in Table 4. The binary system of resid with ANT produced some THF soluble material and insoluble organic material (IOM) in each reaction regardless of resid or atmosphere. The reduced resids showed a higher propensity for having THF soluble materials in the presence of ANT than did the parent resids.

When PHP was added to the resid/ANT system, the change observed was fairly small in terms of the hydrogenation of ANT. However, more hydrogen uptake appeared to be achieved from hydrogen transferred from hydrogen-rich species than from gaseous hydrogen. The %HYD of ANT in N₂ was higher in the systems with PHP present than in those without PHP. Small increases in %HYD were also observed in the hydrogen atmosphere. The product distributions for the ternary systems (Table 4) showed that all of the resids remained toluene soluble. The amount of hexane solubles produced was greater in the hydrogen atmosphere than in the nitrogen for all but one of the systems.

Summary

Hydrogen donation from three types of hydrogen-rich species resulted in substantial hydrogen donation from cyclic olefins, less from hydroaromatic species, and a very small amount from cycloalkanes by comparison. The hydrogen transfer by cycloalkanes to aromatics was promoted by the presence of sulfur. This promotion, however, appeared to be condition specific with more catalysis apparent at 380°C in N₂ than at any other condition. Reduced resids produced by the Birch method were more effective hydrogen donors than their parent resids. Hydrogen enrichment of these resids produced a solvent more effective for the thermal hydrogenation of aromatic species such as are present in coal.

References

- Rudnick, L.R., European Patent 195, 541, 1986a; European Patent 195, 539, 1986b.
Birch, A.J., G.S. Rao, *Advances in Organic Chemistry, Methods and Results*, Vol. 8, E.C. Taylor, ed., Wiley Interscience, NY, NY, 1972.

Table 1. Thermal Reaction Systems

Reaction Conditions	Mole of Hydrogen Released x 10 ⁴		Percent Hydrogenation (%)		Hydrogen Efficiency		Moles of H ₂ From Gas-cous H ₂ Moles X 10 ⁴	
	H ₂	N ₂	H ₂	N ₂	H ₂	N ₂	H ₂	N ₂
	ISO	10.73(0.17)	11.39(0.06)					
ISO/ANT (1:1)	11.08(0.03)	17.00(0.06)	19.24(0.27)	18.32(0.14)	0.39(0.01)	0.24(0.00)	0.21(0.09)	
ISO/ANT (5:1)	44.69(0.61)	45.42(0.13)	24.88(0.07)	24.39(0.18)	0.12(0.00)	0.12(0.00)	0.12(0.05)	
TET	0.05(0.03)	0.03(0.00)						
TET/ANT (1:1)	0.05(0.02)	0.00(0.00)	4.53(0.26)	0.25(0.05)	19.77(2.89)	---	0.96(0.06)	
TET/ANT (5:1)	0.11(0.03)	0.39(0.03)	4.45(0.25)	0.93(0.07)	8.84(1.68)	0.54(0.14)	0.40(0.08)	
PHP	0.00(0.00)	0.00(0.00)						
PHP/ANT (1:1)	0.27(0.02)	0.28(0.05)	3.08(0.28)	0.46(0.17)	2.57(0.22)	0.35(0.09)	0.59(0.08)	
PHP/ANT (5:1)	0.18(0.01)	0.25(0.02)	3.97(0.42)	0.63(0.02)	4.91(0.84)	0.57(0.07)	0.74(0.09)	
ISO/PYR (1:1)	10.99(0.13)	11.80(0.19)	6.02(0.25)	4.11(0.30)	0.08(0.00)	0.05(0.00)	0.28(0.07)	
ISO/PYR (5:1)	49.46(0.79)	47.65(0.32)	17.30(0.27)	13.20(0.75)	0.05(0.00)	0.04(0.00)	0.61(0.15)	
TET/PYR (1:1)	0.00(0.00)	0.00(0.00)	0.00(0.00)	0.00(0.00)	---	---	0.00(0.00)	
TET/PYR (5:1)	0.07(0.00)	0.28(0.19)	0.41(0.09)	0.16(0.01)	0.79(0.18)	0.17(0.12)	0.02(0.01)	
HHA	9.95(0.31)	9.95(0.09)						
HHA/PYR (1:1)	9.93(0.01)	9.52(0.31)	13.59(0.23)	8.14(0.84)	0.20(0.00)	0.13(0.02)	0.81(0.15)	
HHA/PYR (5:1)	35.84(0.48)	43.67(0.82)	30.35(0.97)	10.40(2.48)	0.13(0.01)	0.04(0.01)	2.95(0.50)	
DHA	0.35(0.06)	0.28(0.00)						
DHA/PYR (1:1)	0.43(0.01)	0.52(0.05)	2.46(0.18)	1.63(0.85)	0.87(0.06)	0.44(0.20)	0.15(0.13)	
DHA/PYR (5:1)	1.96(0.03)	1.78(0.19)	11.27(0.35)	8.58(2.17)	0.85(0.04)	0.72(0.17)	0.40(0.37)	

* --- means no hydrogen was released in that condition.

ISO = isotetralin

PHP = perhydropyrene

ANT = anthracene

TET = tetralin

HHA = hexahydroanthracene

DHA = dihydroanthracene

Table 2. Catalytic Reaction Systems

Reaction Conditions	Mole of Hydrogen Released x 10 ⁴		Percent Hydrogenation (%)		Hydrogen Efficiency		Moles of H ₂ From Gas-ous H ₂ Moles X 10 ⁴	
	H ₂	N ₂	H ₂	N ₂	H ₂	N ₂	H ₂	H ₂
380°C Thermal								
PHP/ANT (1:1)	0.27(0.02)	0.28(0.05)	3.08(0.28)	0.46(0.17)	2.57(0.22)	0.35(0.09)	0.59(0.08)	
PHP/ANT (5:1)	0.18(0.01)	0.25(0.02)	3.97(0.42)	0.63(0.02)	4.91(0.84)	0.57(0.07)	0.74(0.09)	
380°C Catalytic								
PHP/ANT (1:1)	0.75(0.01)	0.71(0.16)	4.83(0.53)	0.96(0.14)	1.44(0.18)	0.31(0.91)	0.88(0.14)	
PHP/ANT (5:1)	1.05(0.14)	1.44(0.22)	11.11(0.60)	4.40(0.09)	2.38(0.28)	0.70(0.12)	1.49(0.13)	
440°C Thermal								
PHP/ANT (1:1)	0.24(0.13)	0.55(0.09)	15.44(0.64)	0.30(0.04)	14.13(0.27)	0.13(0.04)	3.40(0.14)	
PHP/ANT (5:1)	0.61(0.13)	0.77(0.15)	15.47(0.16)	2.60(0.19)	5.88(1.27)	0.78(0.15)	2.88(0.07)	
440°C Catalytic								
PHP/ANT (1:1)	0.61(0.03)	0.55(0.27)	14.93(0.19)	1.48(0.13)	5.48(0.30)	0.77(0.49)	3.01(0.09)	
PHP/ANT (5:1)	0.67(0.08)	1.18(0.22)	14.51(0.33)	3.25(0.22)	4.91(0.55)	0.64(0.17)	2.55(0.14)	

PHP = perhydropyrene ANT = anthracene

Table 3. Resid Reaction Systems

Reaction Conditions	Moles of Hydrogen Accepted x 10 ⁴		Percent Hydrogenation (%)		Moles of H ₂ From Gaseous H ₂ Moles X 10 ⁴	
	H ₂	N ₂	H ₂	N ₂	H ₂	H ₂
Maya/ANT (Reduced)	3.15(0.19)	1.62(0.07)	7.03(0.42)	3.61(0.16)	1.52(0.26)	
Maya/ANT (Reduced)	8.02(0.31)	4.26(0.06)	17.90(0.60)	9.50(0.15)	3.76(0.37)	
DAU/ANT (Reduced)	4.69(0.15)	1.61(0.11)	10.03(0.51)	3.59(0.23)	3.07(0.26)	
DAU/ANT (Reduced)	8.31(0.14)	5.08(0.15)	17.94(0.44)	11.34(0.34)	3.22(0.29)	
S.LA/ANT (Reduced)	3.26(0.05)	0.97(0.10)	7.28(0.11)	2.15(0.24)	2.29(0.15)	
S.LA/ANT (Reduced)	5.26(0.07)	3.25(0.17)	11.73(0.17)	7.24(0.38)	2.01(0.24)	
Maya/PHP/ANT (Reduced)	4.98(0.18)	3.09(0.36)	11.10(0.42)	6.90(0.81)	1.88(0.54)	
Maya/PHP/ANT (Reduced)	7.88(0.07)	5.84(0.21)	17.60(0.15)	13.03(0.47)	2.04(0.28)	
DAU/PHP/ANT (Reduced)	4.72(0.23)	3.59(0.09)	10.54(0.52)	8.02(0.21)	1.12(0.32)	
DAU/PHP/ANT (Reduced)	8.08(0.09)	5.85(0.04)	18.02(0.22)	13.06(0.08)	2.22(0.13)	
S.LA/PHP/ANT (Reduced)	3.02(0.17)	1.95(0.14)	6.73(0.38)	4.36(0.31)	1.06(0.31)	
S.LA/PHP/ANT (Reduced)	6.15(0.14)	5.06(0.13)	13.73(0.32)	11.29(0.29)	1.09(0.27)	

DAU = deasphalted resid
 S.LA = South Louisiana resid
 PHP = perhydropyrene
 ANT = anthracene

COAL/OIL COPROCESSING USING SYNGAS :REACTIVITY OF CYCLOALKANES AS THE SOLVENT.

Yuan C. Fu, Kotaro Tanabe, Makoto Akiyoshi
Department of Applied Chemistry,
Muroran Institute of Technology,
Muroran, Japan 050.

Keywords: Coprocessing, Coal, Model Compounds, Syngas

ABSTRACT

Coprocessing of coal or model compounds with petroleum solvents was conducted in the presence of catalysts using syngas (H_2+CO) with steam in place of hydrogen. $NiMo/Al_2O_3$ impregnated with potassium carbonate and $NiMo/MgO$ catalysts exhibited good activities for hydrogenation and desulfurization. High coal conversion was obtained at a mild temperature of 400°C for the coprocessing of coal with petroleum solvents using syngas and steam. With the solvents containing n-paraffin and cycloalkane, it was observed that decalin underwent dehydrogenation and isomerization, and that the extent of hydrodesulfurization increased with the increase of trans/cis ratio of the remaining decalin after the reaction. The presence of aromatic compounds with decalin in the solvent mixtures increased the coal conversion, suggesting that aromatic compounds could be acting as hydrogen shuttlers to transfer hydrogen from decalin to coal.

INTRODUCTION

We have reported previously¹ that coal and model compounds could be hydrogenated and desulfurized in the presence of petroleum solvents and catalyst under coprocessing conditions by using syngas with steam in place of hydrogen. Nickel molybdate on alumina support impregnated with potassium carbonate exhibited good activity with syngas and steam, presumably owing to the simultaneous water-gas shift reaction took place to form active hydrogen. We have continued our quest for catalysts that may also be active in promoting water-gas shift reaction as well as hydrotreating coal in the syngas system. It would be more economical² if syngas could be used in place of expensive hydrogen in coal liquefaction or coprocessing even at the initial stage of two-stage processes.

Another aspect of this investigation is to determine the hydrogen donating ability of cycloalkanes as the solvent in coal/oil coprocessing. It appears that decalin is dehydrogenated and that hydrogen transfer to coal or model compounds takes place under coprocessing conditions. The hydrogen donating ability of decalin is enhanced in the presence of aromatic compounds.

EXPERIMENTAL

The coprocessing reactions of coal and model compounds were conducted in a shaking 25-ml microreactor with syngas ($H_2:CO=1:1$) or H_2 at an initial pressure of 70 kg/cm². The reactor was quickly heated up in a fluidizing sand bath and maintained at 400°C for 45 minutes, and then rapidly quenched in a cold water bath. The catalysts used include a commercial $NiMo/Al_2O_3$ catalyst (Nippon Mining Co.) containing 12.0% MoO_3 and 2.8% NiO , a MgO supported $NiMo$ catalyst containing 12.0% MoO_3 and 4.0% NiO . For syngas runs, the $NiMo/Al_2O_3$ catalyst was impregnated with 10% K_2CO_3 .

Anthracene and benzothiophene were used as the model compounds, and mixtures of n-paraffin, cycloalkane, and aromatic compound were used as petroleum solvents. The ratio of solvent to model compounds was 5:1. For experiments using syngas, 10 weight % of H_2O based on the total amounts of the model compounds and solvent (roughly equivalent to $H_2:CO:H_2O=1:1:0.5$ in the gas phase) was added. In all runs the amount of ground catalyst powders charged was also 10 weight %.

Table 4. Product Distribution from the Resid in Binary and Ternary Systems

Reaction System	Product Distribution, wt%											
	H ₂						N ₂					
	HEX Solubles (%)	TOL Solubles (%)	THF Solubles (%)	IOM (%)	HEX Solubles (%)	TOL Solubles (%)	THF Solubles (%)	IOM (%)	TOL Solubles (%)	THF Solubles (%)	IOM (%)	
Maya/ANT		98.8(0.2)	1.3(0.2)	0.0(0.0)		97.9(1.2)	1.8(1.2)	0.3(0.1)		95.5(0.4)	3.6(1.1)	0.4(0.6)
Maya/ANT (Reduced)		98.2(0.2)	1.4(0.1)	0.4(0.0)								
DAU/ANT		96.9(0.3)	2.9(0.2)	0.2(0.1)		99.1(0.4)	0.9(0.4)	0.1(0.0)		96.9(2.0)	2.9(2.0)	0.2(0.1)
DAU/ANT (Reduced)		96.3(0.6)	3.5(0.6)	0.2(0.1)								
S.LA/ANT		98.7(0.3)	1.1(0.1)	0.2(0.1)		98.2(1.1)	1.7(1.0)	0.1(0.1)		98.6(0.5)	1.4(0.5)	0.0(0.0)
S.LA/ANT (Reduced)		98.4(0.7)	1.5(0.6)	0.2(0.1)								
Maya/ANT/PHP	76.8(1.2)	23.2(1.2)	0.0(0.0)	0.0(0.0)	73.7(0.9)	26.3(0.9)	0.0(0.0)	0.0(0.0)		81.9(0.0)	18.1(0.0)	0.0(0.0)
Maya/ANT/PHP (Reduced)	78.1(2.1)	21.9(2.1)	0.0(0.0)	0.0(0.0)	81.9(0.0)	18.1(0.0)	0.0(0.0)	0.0(0.0)				
DAU/ANT/PHP	81.1(1.4)	18.9(1.4)	0.0(0.0)	0.0(0.0)	76.5(0.6)	23.4(0.6)	0.0(0.0)	0.0(0.0)		83.0(0.3)	17.0(0.3)	0.0(0.0)
DAU/ANT/PHP (Reduced)	88.4(6.1)	11.6(6.1)	0.0(0.0)	0.0(0.0)	83.0(0.3)	17.0(0.3)	0.0(0.0)	0.0(0.0)				
S.LA/ANT/PHP	100.0(0.0)	0.0(0.0)	0.0(0.0)	0.0(0.0)	100.0(0.0)	0.0(0.0)	0.0(0.0)	0.0(0.0)		100.0(0.0)	0.0(0.0)	0.0(0.0)
S.LA/ANT/PHP (Reduced)	100.0(0.0)	0.0(0.0)	0.0(0.0)	0.0(0.0)	100.0(0.0)	0.0(0.0)	0.0(0.0)	0.0(0.0)		100.0(0.0)	0.0(0.0)	0.0(0.0)

DAU = deasphalted resid
 S.LA = south Louisiana resid
 PHP = perhydropyrene
 ANT = anthracene

For coal runs, Illinois No. 6 bituminous coal with an ultimate analysis of C 78.3, H 5.4, N 1.32, O 11.12, S 3.86 (maf basis), ash 10.9% and Wandoan coal with C 67.5, H 5.3, N 0.9, O 15.3, ash 10.9 (mf basis) were used. The ratio of solvent to coal was 2.3:1. The coal conversion was determined from tetrahydrofuran insolubles, and the solubles were analyzed by a gas chromatograph using OV-1701 fused silica capillary column.

RESULTS AND DISCUSSION

Coprocessing Using Syngas. In general, the hydrogenation and hydrodesulfurization activities are somewhat lower with the use of syngas than with hydrogen. It is probably due to the lower partial pressure of H_2 and the existence of other components such as H_2O , CO , and CO_2 in the gas phase. Table 1 shows that the hydrogenation and hydrodesulfurization activities with $NiMo/Al_2O_3$ catalyst are somewhat reduced when the initial H_2 pressure is reduced from 70 kg/cm^2 to 35 kg/cm^2 . Using syngas (without adding H_2O), we observe some decrease of hydrodesulfurization activities even at the same H_2 partial pressure of 35 kg/cm^2 . With syngas, it is postulated that CO may compete with H_2 for active sites and be adsorbed on the catalyst surface. When H_2O is added, the H_2O vapor adsorbed on the surface may poison the catalyst. Therefore, it is presumably important that, for coprocessing using syngas, a suitable catalyst is used and an adequate amount of H_2O is added to promote the formation of active hydrogen via water-gas shift reaction. As was observed previously¹, the extent of the isomerization of decalin increased with the extent of hydrogenation and hydrodesulfurization. Clarke et al² also reported the occurrence of isomerization to trans-decalin during extraction of coal using decalin as solvent.

Hydrogen Donation by Decalin. In order to find out the circumstances at which the isomerization of decalin occurs, trans-decalin and cis-decalin alone were solely hydrotreated under H_2 pressure at 400°C in the presence of $NiMo/Al_2O_3$ catalyst. The results in Table 2 show that 30.4% of cis-decalin and 7.7% of trans-decalin are isomerized, respectively. When the decalin containing both isomers at the trans/cis ratio of 1.6 was hydrotreated under the similar condition, the trans/cis ratio increased to 2.4. It is evident that decalin tends to isomerize from cis-form to trans-form under the hydrotreating condition. However, in the presence of reactants (anthracene and benzo thiophene), the extent of isomerization of cis-decalin solvent increased to 47.8%. On the other hand, only 7.8% of trans-decalin isomerized, indicating the difficulty for trans-decalin to isomerize to cis-form. It appears that both cis- and trans-decalin undergo dehydrogenation (to form tetralin) and hydrogen transfer equally, but the tetralin formed probably forms trans-decalin preferentially as it is rehydrogenated. In fact, an experiment hydrotreating tetralin yielded trans-decalin preferentially (Table 2). With decalin containing both isomers as the solvent, in the presence of reactants, the trans/cis ratio after the reaction was also higher, 4.6 compared to 2.4 (see Tables 1 and 2). Coprocessing experiments using syngas with cis- and trans-decalin solvents also showed that the isomerization to trans-form was favored, but the extent of isomerization was lower.

$NiMo/MgO$ Catalyst. In the quest for catalysts that may be active in the H_2 - CO - H_2O system, a $NiMo/MgO$ catalyst was prepared and tested. The results in Table 3 show that $NiMo/MgO$ catalyst exhibits comparable activities with $NiMo/Al_2O_3$ catalyst for coprocessing of model compounds. In the syngas system, the alkaline MgO was able to promote CO conversion and no impregnation with K_2CO_3 was necessary. Of various catalysts tested, including synthetic pyrite, $ZnCl_2/SiO_2-Al_2O_3$, Fe_2O_3/SO_4^{2-} , cobalt molybdate, and nickel molybdate, $NiMo$ catalysts with various characteristics of supports may be the most interesting area to explore.

Coprocessing of Coal with Petroleum Solvents. Table 4 shows the experimental results of coprocessing Illinois No. 6 coal and Wandoan coal with petroleum solvents. At the mild temperature of 400°C, $NiMo/Al_2O_3$ catalyst impregnated with K_2CO_3 exhibited good activities with syngas, and high coal conversions obtained were comparable to those obtained with hydrogen. At temperatures greater than 425°C, because of lower H_2 partial

pressures with syngas, the fragments from thermally decomposed coal tend to polymerize to form char. The experimental runs using NiMo/MgO catalysts show that coal conversions were somewhat lower with either H₂ or syngas.

It was also observed that hydrogen donating properties of paraffin-cycloalkane solvent mixtures were enhanced by the presence of cyclic compounds containing benzene rings such as tetralin and 1-methylnaphthalene. Even though 1-methylnaphthalene is not a hydrogen donor, its addition to the dodecane-decalin mixture increased the coal conversion, equivalent to that obtained with the addition of tetralin (see Table 4). This suggests that aromatic compounds, in paraffin-cycloalkane solvents, may act as hydrogen shuttlers to transfer hydrogen from cycloalkane to coal.

ACKNOWLEDGEMENTS

We thank the support of Grant-in-Aid of Scientific Research provided by the Ministry of Education, Japan. We also thank Nippon Mining Co. for providing catalyst samples.

References

1. Fu, Y.C., Akiyoshi, M., Tanaka, F., Fujiya, K., Preprints. Div. Fuel chem., Am.chem.soc. Vol 36, No.4, 1887 (1991)
2. Batchelder, R.F., Fu, Y.C., Ind.Eng.Chem. Process Des. Dev. Vol.18, No.4, 599 (1979)
3. Clarke, J.W., Rantell, T.D., Snape, C.E., Fuel, Vol.63, 1476 (1984)

Table 1 Coprocessing of Model Compounds with Petroleum Solvents
(Catalyst: NiMo/Al₂O₃, Reaction temp.: 400°C, Time: 45min)

Gas	H ₂		Syngas	Syngas+H ₂ O ^a
	kg/cm ²	DO/DL		
Initial pressure	70	35	70	70
Solvent ^b	DO/DL	DO/DL	DO/DL	DO/DL ^c
Anthracene conv. %	89.4	65.3	63.1	90.6
Benzothiophene conv. %	100	80.0	71.6	52.6
Decalin remained. %	76.2	66.5	88.5	75.3
cis	13.7	15.5	62.5	47.0
trans	62.5	51.0	26.0	28.3
trans/cis ratio	4.6	3.3	2.4	0.6
CO conv. %	-	-	13.1	35.2

DO: Dodecane, DL: Decalin

a) NiMo/Al₂O₃ impregnated with K₂CO₃

b) Equal wt% of each component

c) 100% cis-Decalin

Table 2 Coprocessing Using Decalin Isomers as Solvents
(Initial Pressure: 70 kg/cm², Temperature: 400°C, Time: 45min)

Gas	H ₂					Syngas+H ₂ O		
	NiMo/Al ₂ O ₃					NiMo-K ₂ CO ₃ /Al ₂ O ₃		
Catalyst	c-DL	DO/c-DL	t-DL	DO/t-DL	DO/DL	T	DO/c-DL	DO/t-DL
Solvent	-	A, B	-	A, B	-	-	A, B	A, B
Model compound	-	A, B	-	A, B	-	-	A, B	A, B
A conv. %	-	98.5	-	98.9	-	-	90.6	83.0
B conv. %	-	94.9	-	94.3	-	-	52.6	46.5
EB formed. %	-	69.3	-	62.8	-	-	19.1	23.5
Decalin remained. %	96.1 ^a	94.7	98.9 ^a	82.3	92.4	11.0 ^b	75.3	87.0
cis	65.7	46.9	7.7	7.8	27.4	2.8	47.0	6.4
trans	30.4	47.8	91.2	74.5	65.0	8.2	28.3	80.5
trans/cis ratio	0.46	1.0	11.8	9.6	2.4	2.9	0.6	12.5
CO conv. %	-	-	-	-	-	-	35.2	28.7

c-DL: cis-Decalin, t-DL: trans-Decalin, DO: Dodecane, T: Tetralin

A: Anthracene, B: Benzothiophene, EB: Ethylbenzene

a) The remainder converted to tetralin.

b) Decalin formed, Tetralin remained is 84.2%, and the remainder converted to naphthalene.

Table 3 Coprocessing of Model Compounds on NiMo Catalysts
(Solvent:n-Decane/Decalin/Tetralin, Initial Pressure:70 kg/cm².
Temp.:400°C. Time:45min)

Catalyst	H ₂		Syngas+H ₂ O	
	NiMo/Al ₂ O ₃	NiMo/MgO	NiMo/Al ₂ O ₃ ^a	NiMo/MgO
Anthracene conv.,%	100	100	96.1	99.2
Benzothiophene conv.,%	100	100	93.9	100
Ethylbenzene formed, %	80.5	78.8	83.7	88.3
H ₂ consumption, % ^b	7.0	5.1	0.3	-0.5
CO conv., %	-	-	37.2	40.6
Decalin remaind, %	116.4	85.5	92.5	96.3
cis	27.2	24.5	26.7	27.3
trans	89.2	61.0	65.8	69.0
trans/cis ratio	3.3	2.5	2.5	2.5
Tetralin conv., %	34.4	24.4	12.2	19.0
Naphthalene formed, % ^c	6.8	3.8	4.1	9.3

- a) Impregnated with K₂CO₃
b) Wt. % of coal models
c) Based on the initial amount of tetralin

Table 4 Coprocessing of Coals with Petroleum Solvents at 400°C

Gas	H ₂				Syngas (H ₂ :CO=1:1)			
	NiMo/Al ₂ O ₃		NiMo/MgO		NiMo/Al ₂ O ₃ ^a		NiMo/MgO	
Solvent	DO/DL/T	DO/DL/MN	D/DL/T	D/DL/T	DO/DL/T	DO/DL/MN	D/DL/T	D/DL/T
Coal conversion, %	89.0 ^b	86.5 ^b	89.9 ^c	76.7 ^c	87.9 ^b	85.5 ^b	87.3 ^c	74.8 ^c
H ₂ consumption, wt% of maf coal	3.9	4.5	5.5	2.3	0.9	0.9	-1.3	-0.2
CO conv., %	-	-	-	-	7.3	12.0	46.0	28.5
Decalin remained, %	98.1	89.9	88.4	96.6	95.8	94.3	85.3	97.9
cis	33.7	29.8	33.7	36.5	33.3	34.5	31.9	36.9
trans	64.4	60.1	54.7	60.1	62.5	59.8	53.4	61.0
trans/cis ratio	1.9	2.0	1.6	1.6	1.9	1.7	1.7	1.7
Tetralin conv., %	2.3	10.3 ^d	3.5	0.3	11.1	7.7 ^d	17.1	1.0

D:n-Decane, DO:Dodecane, DL:Decalin, T:Tetralin, MN:1-Methylnaphthalene

- a) Impregnated with K₂CO₃ solution
b) Illinois No.6 coal
c) Wandoan coal
d) Conversion of 1-Methylnaphthalene

Nanoscale Fe-based Catalysts from Laser Pyrolysis

P. C. Eklund, Xiang-Xin Bi, and F. J. Derbyshire
Center for Applied Energy Research
University of Kentucky
Lexington, KY 40511-8433

Keywords: Ultrafine particle, catalyst, coal liquefaction, laser pyrolysis

Introduction

Iron-based catalysts have been extensively investigated for their catalytic behavior in direct coal liquefaction^[1]. Although they are generally less active than other catalysts containing transition metals such as molybdenum, vanadium, etc, they are favored for economical reasons. The catalytic activity of these iron-based catalysts depends mainly on their chemical composition and effective contact area with the coal-solvent slurry. The contact area relates closely to the particle diameter, surface morphology, and particle agglomeration. Research to produce nanoscale (~10 nm dia.) ultrafine particle (UFP) catalysts with *controllable* chemical composition and particle size is of fundamental importance to study the effect of these factors on the catalytic activity.

In this paper, we report the results of a study to synthesize and characterize nanoscale (5-20nm) UFP Fe-based catalysts for direct coal liquefaction. The UFPs were produced by the laser-driven gas phase reaction of $\text{Fe}(\text{CO})_5$ with C_2H_4 . By adjusting the reaction conditions we have found it possible to produce reasonably pure phase (~95%) batches of $\alpha\text{-Fe}$, Fe_3C and Fe_7C_3 particles with a size distribution of ~2-4 nm. Typical production rates are ~1 g/hr. By adding H_2S to the reactant gas stream we have succeeded recently in producing UFP pyrrhotite (Fe_{1-x}S). Results from our studies to determine the catalytic benefit of UFP Fe-carbide catalysts in coal liquefaction have produced some promising results^[2]. These experiments were carried out in a microautoclave with dimethyl disulfide (DMDS) added to improve conversion to iron sulfide. Our studies have shown that, under liquefaction conditions, the UFP Fe-carbide catalysts are transformed into pyrrhotite. This transformation complicates the identification of the active catalyst phase and, of course, raises questions about the activity and the role of the carbides in the conversion of coal into liquids and gases. Our recent success in synthesizing UFP pyrrhotite should allow us to study these questions, as well as evaluate the activity of UFP Fe_{1-x}S .

We have characterized the physical properties of our UFP catalysts by X-ray diffraction (XRD), optical spectroscopy (reflectivity and Raman scattering),

transmission and scanning electron microscopy (TEM and SEM) and ^{57}Fe Mossbauer spectroscopy.

The CO_2 laser pyrolysis technique, invented by Haggerty et al.^[3], has been established as a useful technique for the synthesis of ultrafine particles (UFP) in the size range 5 - 30 nm. In the past, a variety of UFPs have been produced using this technique; they include $\{\text{Si}, \text{SiC}, \text{Si}_3\text{N}_4\}$ ^[3], $\{\text{ZrB}_2, \text{TiO}_2\}$ ^[4], Fe_3C ^[5], $\{\text{WC}, \text{MoS}_2\}$ ^[6]. These UFPs (e.g., SiC and Si_3N_4) have been found to be free from contamination and exhibit a narrow particle size distribution^[3]. The synthesis of UFP Fe_3C using laser pyrolysis was first explored by Fiato et al. at Exxon^[5]. They proposed a basic chemical reaction involving the thermal decomposition of $\text{Fe}(\text{CO})_5$ and subsequent reaction with C_2H_4 at high temperature sustained by CO_2 laser illumination which couples strongly to the vibrational bands of C_2H_4 . They found that UFP Fe_3C forms as a product of this process. Fiato et al.^[5] demonstrated that the particle composition, i. e., carbon to iron ratio, could be controlled by varying the preparation conditions. Prior to our work, no studies have been reported which correlate the reaction parameters with particle size, chemical composition or crystalline phase. Furthermore, the Exxon group did not report the formation of Fe_7C_3 , which exhibits a hexagonal structure^[12].

Experiment

Our laser pyrolysis system^[3-5, 7, 8] is shown schematically in Fig. 1. The reactant gases flow vertically out of a stainless steel tube with a nozzle of area A. Studies of the effect of A on particle production have been carried out over the range $A \sim 2 - 5 \text{ mm}^2$. The pyrolysis reaction zone is formed at the intersection of the horizontal infrared beam from a continuous (CW) CO_2 laser, tuned at the P20 line, and the vertical flow of reactant gases from the nozzle. The reactant gases and associated particle growth are confined within the reaction zone by a coaxial flow of Ar gas which passed through a larger tube concentric with the much smaller reactant gas tube (Fig. 1). Argon gas is also introduced into the entrance and exit windows in such a way as to continually sweep any stray particles off the NaCl windows (Fig. 1). Mass flow controllers are used to establish steady gas flows of Ar, and to regulate the flow of C_2H_4 (2-30 sccm) and H_2S (2-20 sccm). The total pressure in the cell was controlled by a needle valve located between a rotary vacuum pump and the stainless steel reaction chamber (6-way cross). Particles are collected downstream in a Pyrex trap indicated in Fig. 1. Since the $\alpha\text{-Fe}$, Fe_3C and Fe_7C_3 particles are ferromagnetic, we have employed a magnetic field to trap the particles using a stack of permanent magnets placed beneath the trap (Fig. 1).

The pyrrhotite Fe_{1-x}S UFPs were synthesized by adding H_2S to the C_2H_4

and $\text{Fe}(\text{CO})_5$ reactant gas stream, at a flow rate of 7 sccm. The other reaction parameters are set at the values which would otherwise produce α -Fe particles (Table 1). These sulfide particles are non-magnetic and are not attracted to the magnets beneath the collection trap (Fig. 1). As a result, the particles tend to drift toward the far end of the trap and clog the 0.2μ pore size membrane filter, which complicates the steady state production of these particles. Other means of trapping pyrrhotite particles are being investigated to solve this problem. It is interesting to speculate that the non-magnetic properties of pyrrhotite UFPs may lead to much less particle agglomeration compared to ferromagnetic carbide UFPs, and thus better dispersion in the coal slurry.

To handle most of our Fe-based UFPs in air, we have found it necessary to passivate the surface in situ in the collection trap. The passivation is carried out by flowing 4-10% O_2 -in- He_2 for several hours.

Results and Discussion

Shown in Fig. 2 are the XRD results for UFP α -Fe, Fe_3C and Fe_7C_3 using the reaction parameter values given in Table 1. In this figure, the dots represent experimental data and the lines are calculated using a sum of Lorentzian functions whose peak positions and relative strengths are obtained from published powder diffraction data^[9]. The same width parameter is used for all diffraction lines, and an exponential function is introduced to simulate the background. The Debye-Scherrer equation has been used to convert the X-ray line width into an average particle diameter. We find that these X-ray derived values for the particle diameter are in good agreement with Transmission Electron Microscopy (TEM) results, indicating that the UFPs are, for the most part, single crystal particles. The calculated diffraction pattern is seen to agree reasonably well with the data^[9], leading to our identification of the three phases as α -Fe, Fe_3C and Fe_7C_3 . The signature of Fe_3O_4 in the XRD data of α -Fe is believed to stem from the O_2 passivation.

We have found that higher chamber pressures (> 300 torr) and higher reactant gas flow rates (> 30 sccm) favor the formation of high carbon content crystalline phases such as Fe_7C_3 . On the other hand, lower chamber pressures and reactant gas flow rates favor the formation of α -Fe. A detailed study of the correlation between reaction parameter values and the associated solid UFP phases produced will appear elsewhere^[8]. Presented in Fig. 3a and 3b are, respectively, the XRD results for several batches of Fe_3C and Fe_7C_3 particles produced with different average particle sizes. The particle size indicated in the figure was estimated using the Debye-Scherrer equation^[13] and the data near $2\theta \sim 58^\circ$.

In Fig. 4, we show ^{57}Fe Mossbauer spectra collected at 12K for both Fe_3C and Fe_7C_3 . The solid line in Fig. 4 represents the calculated Mossbauer spectrum by fitting the data in the usual way. The results from the fit to room temperature data including internal magnetic field, isomer shift and quadruple splitting parameters are listed in Table 2. The parameter values for the Fe_3C particles at room temperature^[8] are compared with the results of Le Caer et al.^[11], and are found to be in good agreement. To our knowledge, Mossbauer results for Fe_7C_3 have not been reported. We find in this study that a model with four inequivalent magnetic sites is necessary to fit the data. Fe_7C_3 has three chemically inequivalent sites^[10]. Further Mossbauer and neutron scattering studies are underway to determine the magnetic structure of Fe_7C_3 UFPs.

Shown in Fig. 5 by the dotted lines are XRD data for iron sulfide (pyrrhotite) UFPs. For comparison, the solid lines in the figure represent the XRD data of Fe_7C_3 particles after reaction in our microautoclave with dimethyl disulfide(DMDS) at 375 °C. The vertical lines represent the standard powder diffraction intensities for pyrrhotite. As can be seen in the figure, the Fe-sulfide UFPs exhibit a diffraction pattern quite similar to pyrrhotite. However, on the basis of the XRD data, it is not possible to rule out that there may be significant incorporation of carbon into the UFP pyrrhotite lattice. Mossbauer studies are currently underway to address this point. One can also conclude from the XRD data in the figure that liquefaction conditions (and the presence of DMDS) rapidly converts UFP Fe-carbide into UFP pyrrhotite with slightly smaller particle size (and possibly with significant carbon content).

New results from coal liquefaction studies using nanoscale Fe-based catalysts, including UFP-pyrrhotite, will also be presented.

Acknowledgement

We thank Bhaswati Ganguly, Dr. Frank E. Huggins and Dr. Gerald P. Huffman for the Mossbauer studies. This work is supported by DOE Advanced Concepts, DE-AC22-91PC91040.

References

1. Derbyshire, Frank J., *Catalysis in Coal Liquefaction: New Direction for Research*(1988) IEA Coal Research, p. 2
2. Hager, Bi, Derbyshire, Eklund, Stencil, "Ultrafine Iron Carbide as Liquefaction Catalyst Precursor", ACS Preprints- Division of Fuel Chemistry, 36(4) 1900-8(1991)
3. J. S. Haggerty, *Sinterable Powders from Laser-Driven Reactions*, in *Laser-induced Chemical Processes*, J.I. Steinfeld, Editor. 1981, Plenum Press: New York.
4. G. W. Rice, and R. L. Woodin, J. Am. Ceram. Soc., 1988. 71 : p. C181.
5. R. A. Fiato, G. W. Rice, S. Miseo, and S. L. Soled, United States Patent, 1987. **4,637,753**.
6. R. A. Fiato, G. W. Rice, and S. L. Soled, U. S. Patents, 1988. **4659681, 4668647**.
7. G. W. Rice, and et al., United States Patent, 1987. **4,659,681**.
8. G. W. Rice, and R. L. Woodin. *Applications of Lasers to Industrial*. in *SPIE*. 1984.
9. Powder Diffraction File of the Joint Committee on Powder Diffraction Standard(International Center for Diffraction Data, Swarthmore, PA, 1991).
10. Xiang-Xin Bi, P. C. Eklund, et al., in preparation.
11. R. L. Cohen, *Applications of Mossbauer Spectroscopy*. ed. R.L. Cohen, 1980, New York: Academic Press.
12. H. L. Yakel, International Metals Reviews, 1985. **30**: p. 17.
13. B. D. Cullity, *Elements of X-Ray Diffraction*. 1967, Addison-Wesley Publishing Company, Inc.

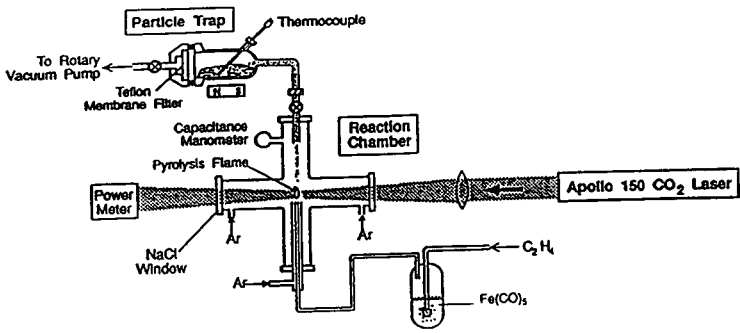
Table 1 Typical laser pyrolysis reaction parameters.

	α -Fe	Fe ₃ C	Fe ₇ C ₃
Laser Intensity(W)	30	50	54
Beam Width(mm)	1	1	0.2
Nozzle Diameter(mm)	1.7	0.8	0.8
Chamber Pressure(Torr)	100	300	500
C ₂ H ₄ Flow Rate(sccm)	9	9	25

Table 2 Room-temperature ⁵⁷Fe Mossbauer parameters including hyperfine magnetic splitting(H₀), isomer shift(I. S.) and quadropole splitting(Q. S.) for UFP Fe₃C and Fe₇C₃.

	H ₀ (KG)	I. S. (mm/s)	Q. S. (mm/s)
Fe ₇ C ₃ *	228	0.32	-0.17
	210	0.23	0.03
	185	0.20	-0.04
Fe ₃ C*	163	0.21	0.07
	210	0.19	0.02
Fe ₃ C ⁽¹¹⁾	198	0.19	0.01
	208	0.18	0.02
	206	0.18	0.02

* present work.



**UFP Production
by Laser Pyrolysis**

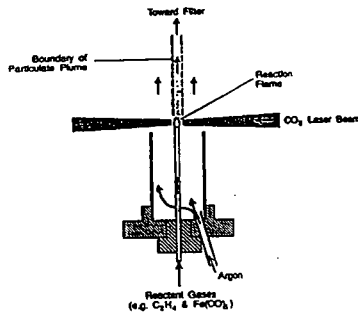


Fig. 1 Laser pyrolysis system for the synthesis of ultrafine iron carbide and sulfide particles.

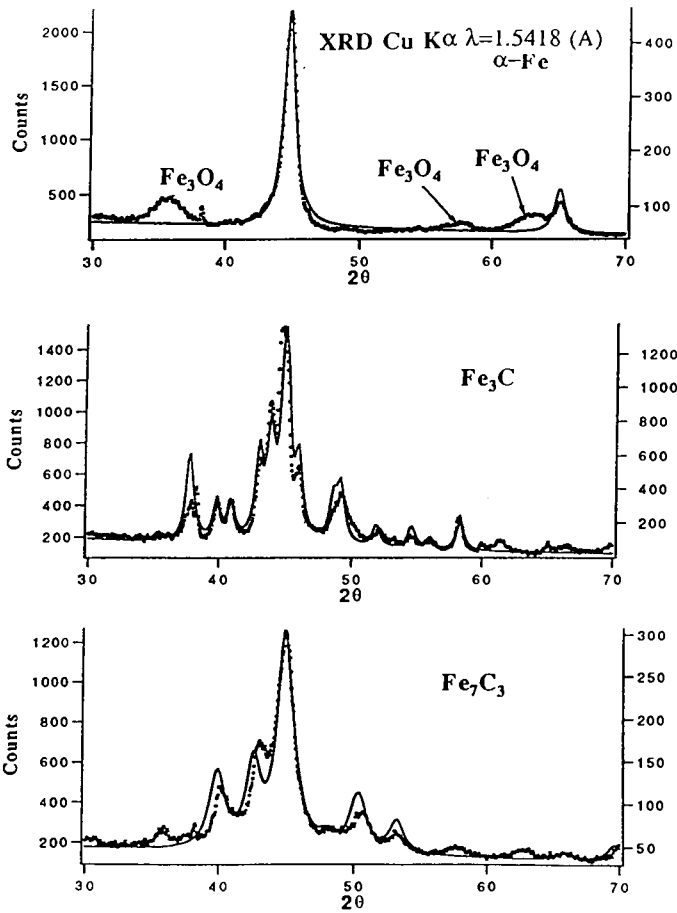


Fig. 2 XRD data(dots) for $\alpha\text{-Fe}$, Fe_3C and Fe_7C_3 UFPs and calculated results (solid curves) using standard diffraction data^[9] with an exponential background.

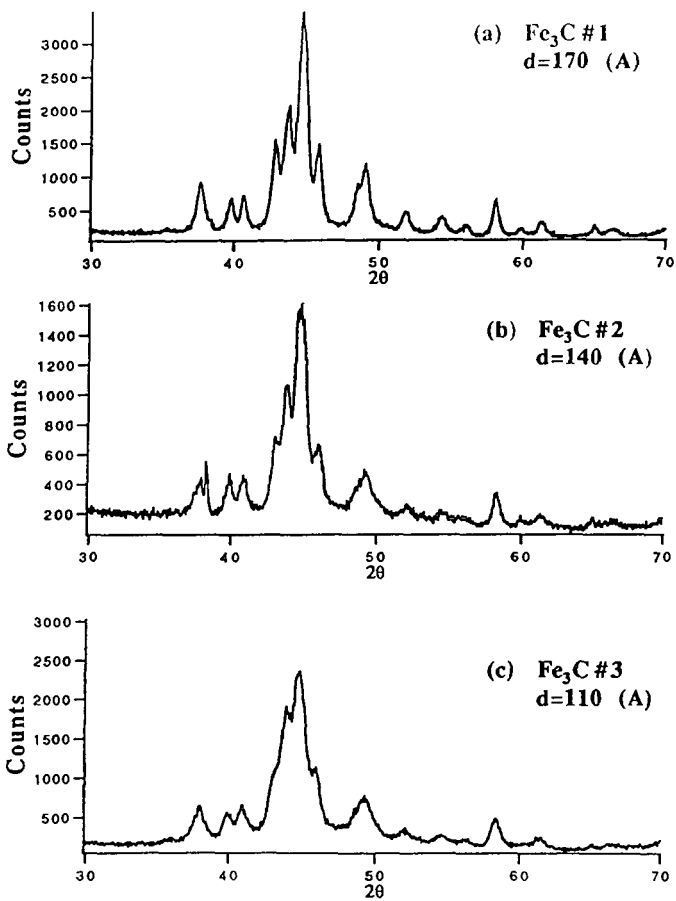


Fig. 3(a) XRD data for Fe_3C UFPs of different particle size.

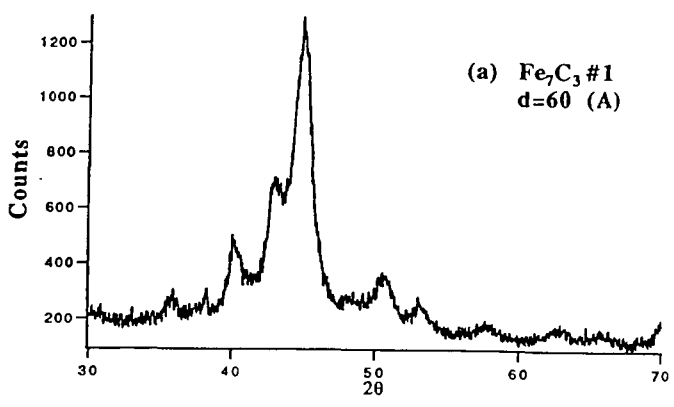
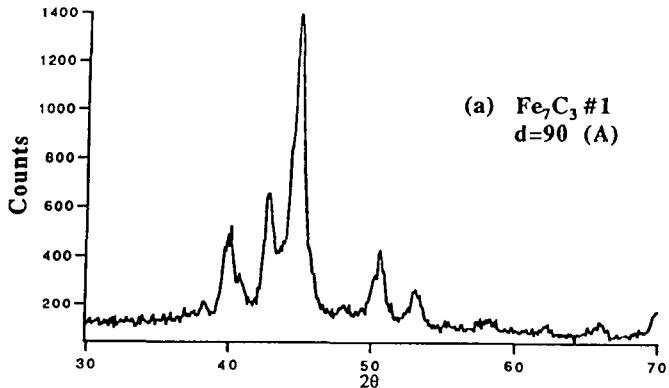


Fig. 3(b) XRD data for Fe_7C_3 UFPs of different particle size.

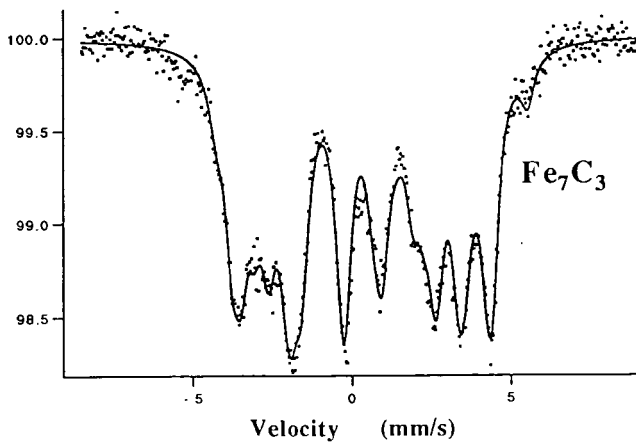
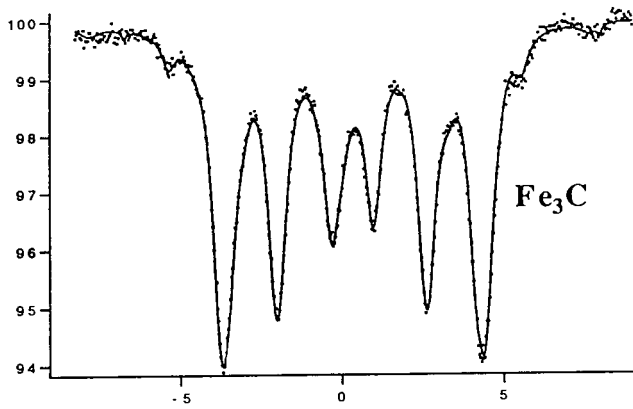


Fig. 4 ^{57}Fe Mossbauer spectra(dots) at $T=12\text{ K}$ for Fe_3C and Fe_7C_3 . Solid lines are calculated using a set of parameters that fit the data.

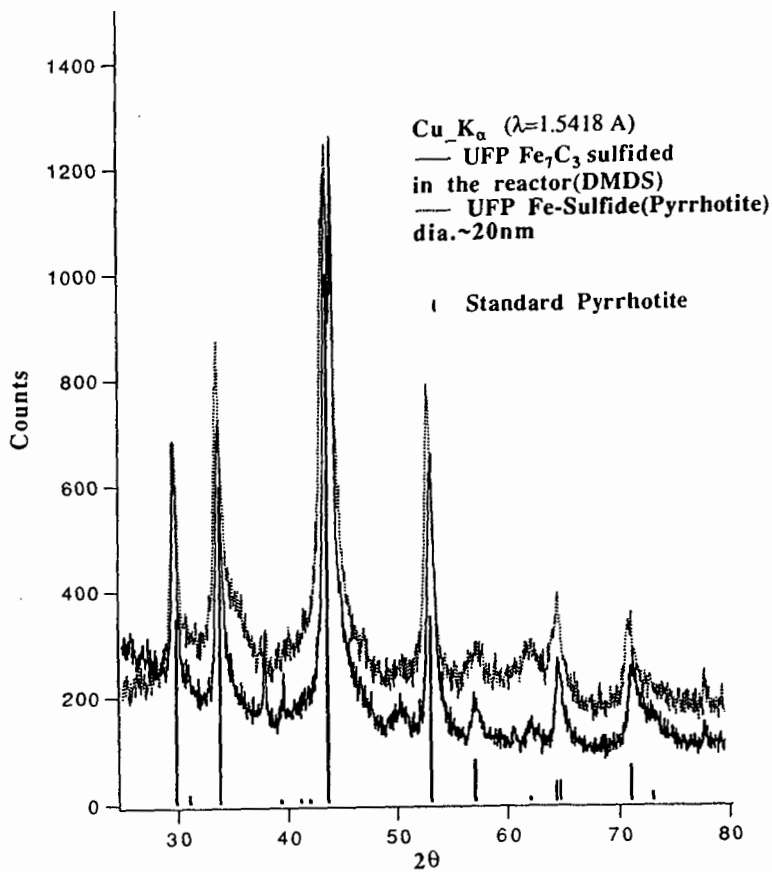


Fig. 5 Dotted lines are XRD results for the pyrrhotite Fe_{1-x}S UFPs obtained by using laser pyrolysis, and solid lines by sulfiding iron carbide Fe₇C₃ UFPs with DMDS at 375 °C(solid lines). The vertical lines represent standard powder diffraction data^[9] for Fe_{1-x}S phase.

CONVERSION OF RESID COMPONENTS IN CC-ITSL PROCESSING AT WILSONVILLE

G. A. Robbins, R. A. Winschel, F. P. Burke
CONSOL Inc.
Research & Development
4000 Brownsville Road
Library, PA 15129

Key words: Liquefaction, Resid, Kinetics

INTRODUCTION

Integrated Two-Stage Liquefaction technology has evolved to its current configuration, in which high recycle rates of solids and non-distillable materials contribute to high conversions and distillate yields. At the Wilsonville, Alabama, 6 ton/day pilot plant, the feed stream contains 29-33 wt % coal, 27-34 wt % resid (850°F⁺), and 8-16 wt % cresol insolubles (CI). Only 25-28% of the feed is distillable. In a recent assessment of analytical needs,¹ it was concluded that the chemistry of residual materials is an important area for study, including improved analytical methods for resid characterization and more extensive kinetic modeling. CONSOL has characterized process oils from each of the last nineteen Wilsonville runs; Close-Coupled Integrated Two-Stage Liquefaction (CC-ITSL) operation of the plant spanned fifteen runs since 1985. This paper represents an initial attempt to review and refine some areas of our investigations of resid conversion chemistry in Wilsonville runs.

EXPERIMENTAL

The experimental methods used in the analysis of whole process oils were reported elsewhere in detail.^{2,4} A brief description is provided here. Each whole process oil is distilled to 850°F to produce a distillate and a resid. Tetrahydrofuran (THF) solubles are obtained by repeated washing of distillation bottoms with distilled THF and recovery by rotary evaporation. Phenolic -OH concentration in the THF-soluble resid is determined by Fourier Transform infrared spectroscopy in THF solution. The THF-soluble resid is fractionated successively into oils (hexane-solubles), asphaltenes (benzene-solubles), and preasphaltenes (pyridine-solubles) with analytical quantitation by flame ionization detection (using different response factors for each feed coal represented). Each insoluble resid fraction is ashed at 800°C to constant weight and insoluble organic matter (IOM, also referred to as unconverted coal, or UC) is determined by difference between weights of ash and THF-insolubles.

The process oils analyses are used to calculate conversions (forced ash balance method) of the 850°F⁺ material and its various components in each reactor stage. The 850°F⁺ conversions are used to calculate conversion rate constants, conversion activities, and a catalyst deactivation rate constant.⁵ Equations used are:

$$C = \text{Conversion} = \left(\frac{850^{\circ}\text{F}^+ \ln/\text{Ash In} - 850^{\circ}\text{F}^+ \text{Out}/\text{Ash Out}}{850^{\circ}\text{F}^+ \ln/\text{Ash In}} \right) \times 100\%$$

$$K = \text{Rate Constant} = \text{WHSV} \left(\frac{C}{100 - C} \right)$$

$$A = \text{Conversion Activity} = K_0 E_{\text{act}} / RT$$

where E_{act} is assumed to be 23,500 cal/mol. In addition to conversion of the total 850°F⁺ resid, it is possible to calculate conversion of any component, including IOM, THF-solubles, oils, asphaltenes, preasphaltenes, and phenolic -OH.

RESULTS AND DISCUSSION

Background Table 1 summarizes the major operating conditions for CC-ITSL Runs 257 through 262. Generally several significant differences exist among runs. Detailed discussions of each run have been reported by Wilsonville⁶ and CONSOL⁷. A block diagram of the Wilsonville plant appears in Figure 1.

Comparison of CONSOL and Wilsonville Distillation Procedures and Resid Conversions. CONSOL uses an 850°F atmospheric equivalent distillation endpoint; the Wilsonville laboratory uses a 1050°F endpoint.⁵ Therefore, the 850 x 1050°F boiling fraction is considered resid in CONSOL's analyses, but distillate in Wilsonville's analyses. Table 2 illustrates this. On average, CONSOL typically measured about 14 wt % more resid than did Wilsonville. The amount of the difference may be related to reactor volume either directly or indirectly (see Table 2). Because of the difference, conversions calculated from CONSOL data are of 850°F⁺ material; Wilsonville's conversions are of 1050°F⁺ material. Some implications of this difference have been discussed elsewhere.⁵

One way to compare the (850°F⁺) conversions obtained by CONSOL with those obtained by Wilsonville (for 1050°F⁺) is to calculate the CONSOL/Wilsonville conversion ratio (R(C/W)) (Figure 2). Several observations were made from these data. First, R(C/W) averaged 0.8-1.0 in most runs, indicating CONSOL conversions were generally somewhat lower than Wilsonville conversions. Second, the R(C/W) ratio did not correlate with CONSOL and Wilsonville values for V-131B resid content (Table 2). Third, Run 262 was unprecedented in the low R(C/W), in each stage (not shown) and total system. It is not obvious why the 850 x 1050°F conversion was so low relative to the conversion of 1050°F⁺ material, but perhaps paraffinic components present in the 850 x 1050°F fraction were not readily converted to distillate in Run 262. Several points can be made regarding this: 1) Wilsonville found significant quantities of waxes in the Run 262 distillate products, and experienced unprecedented handling problems with them. 2) CONSOL found the heavy distillate paraffinity to be very high in Run 262. 3) The Run 262 resid alkyl beta protons were high, but not unprecedented; they were consistently this high only in one other CC-ITSL run (Run 257). How these results may be related to the use of Molyvan L (dispersed catalyst precursor first used in Run 262) is unknown. Perhaps dispersed Mo is not a good paraffin cracking catalyst, or the high coal space velocity during Run 262 was a contributor to poor cracking.

Corresponding first- and second-stage results are not shown, but are summarized here. R(C/W) for the first stage (typically slightly lower than one) in any given period is usually greater than that of the second stage (typically 0.8). These observations seem consistent with the first stage conversion which is dominated by IOM, and is not highly subject to variation in distillation conditions. The conversion of material in the second stage is more sensitive to distillation conditions and shows a greater difference in CONSOL and Wilsonville results. There was more scatter in the second-stage ratios.

Catalyst Deactivation in Run 258. Kinetic rate constants and activities (pre-exponential factors) for 850°F⁺ conversion were calculated for Run 258 material balance periods to evaluate catalyst activity and deactivation. In many recent runs, a look at catalyst deactivation was impossible because most operating periods were obtained at similar (equilibrium) catalyst ages. However, tests at several catalyst ages (some were from batch aging) in Run 258 allowed a catalyst activity evaluation. In order that the calculation would not be skewed by many data points near the equilibrated age of ca. 2500 lb (resid + C)/lb cat, all of those data (periods B through F, H, and I) were averaged to a single value (transitional periods were omitted). The deactivation rate constant is evaluated by considering the conversion activity, A, to have an exponential dependence on catalyst age, t, as $A = A' e^{-\alpha t}$, where A' is the initial conversion activity. As written, catalyst deactivation will result in negative values of α , the deactivation rate constant. The value of α was determined by regression of $\ln A$ on t. The results (Table 3 and Figure 3) indicate no significant effect of second-stage catalyst age on first-stage activity, as is expected for the thermal first stage (in the absence of any solvent donor effect). However, a deactivation rate constant is obtained for the second-stage catalyst with a high correlation, although for only four data points. The α and A' values for the second-stage catalyst are similar to those CONSOL found for Wilsonville Runs 250 through 257.⁵ However, the correlation of catalyst activity with age in Run 258 was much stronger than in those prior runs.

Conversion of Resid Components. Conversions of components of the 850°F⁺ resid (850°F⁺ resid, THF-solubles, oils, asphaltenes, preasphaltenes, and phenolic -OH) were calculated for Runs 257 through 262 (Figure 5). In Run 262 (Black Thunder coal, see Figure 5a), the resid + IOM conversion was positive in the first stage and low in the second stage, resulting in equivalent first-stage and total conversions. The conversion of THF-soluble resid and its components showed negative first-stage and total conversions, with higher second-stage conversions. The negative conversions represent gains in those components, from conversion of coal to solubles. Second-stage conversions of THF solubles, oils, and asphaltenes were approximately zero, making the corresponding first-stage and total conversions equivalent. Conversions of

preasphaltenes and phenolic -OH differ from those of the other components: they are greater in magnitude, showing greater first-stage and total gains (negative conversions); and the second-stage conversions are large and positive, resulting in increases in the total system conversions. The large negative conversion (net gain) of preasphaltenes in the first stage implies that preasphaltenes are primary coal solubilization products and that they are an intermediate form in the transition from coal to distillate. In the second stage, little additional coal is converted, and the conversion of preasphaltenes to other products is positive. The phenolic -OH conversion shows a similar trend with reactor stage, presumably because preasphaltenes are high in phenolic -OH (but the other fractions contain phenolics, as well). These results suggest that preasphaltenes and/or phenolic -OH could be important to include as a group in lumped kinetic modeling. This could be important in overall evaluations of performance, since heteroatom removal is a significant role of the catalyst, and since refining of the liquids to final products has a major impact on process economics.

Figure 5b shows the average results from Run 261, a catalytic/catalytic, low/high temperature run, with Illinois 6 feed coal. The preasphaltene and phenolic -OH conversions show the same trends as in Run 262. Trends in conversions of resid + IOM and other components somewhat resemble those in Run 262, but a number of differences are evident. In Run 261, the second-stage conversion of resid + IOM was relatively high and contributed a great deal to the total conversion. Conversions of THF-solubles and asphaltenes were positive in the second stage in Run 261, contributing to the respective total conversions. Total conversions of THF-solubles, oils and asphaltenes, and conversion of oils in each stage, were all close to zero. The results for Run 257 (another catalytic/catalytic Illinois 6 coal run) were very similar to those for Run 261, in spite of the fact that Run 257 used a high/low temperature configuration.

Resid component conversion results from two segments of Run 260 (Black Thunder coal) are shown in Figures 5c and 5d. One is thermal/catalytic, high/low operation (periods A-C), and the other is catalytic/thermal, low/high operation (periods D-F). The trends in resid component conversion during thermal/catalytic operation are quite similar to those seen in Run 261 (Figure 5b). Run 260 resembles the other subbituminous thermal/catalytic runs (262 and 258), however, in the relatively low second-stage resid + IOM conversion. That situation changed during catalytic/thermal operation in Run 260 (Figure 5d), when the two reactors more equally shared the contribution to conversion of resid + IOM. Also during catalytic/thermal operation, the first-stage, second-stage, and total conversions of most resid components were approximately zero. The preasphaltene conversions were still the most sensitive, but their magnitude was greatly reduced relative to the other runs discussed. The phenolic -OH conversions were quite small in magnitude, and were close to zero. Overall, it appears as if catalytic/thermal operation in Run 260 nearly balanced the work performed by each reactor and put the reactors into a near-equilibrium situation with respect to resid conversion. Thus, for most components, there was little net conversion or gain. A net conversion of coal to preasphaltenes occurred in the first stage and total system. In the second stage, coal conversion to resid was balanced by resid conversion to distillate.

CONCLUSIONS

In the latest Wilsonville CC-ITSL runs, the first stage primarily converts coal to solubles; conversion of soluble components takes place principally in the second stage. Preasphaltenes (which are high in phenolics) seem to be the primary coal solubilization product, and their conversion is effected primarily in the second stage. Including preasphaltenes and/or phenolic -OH components in lumped kinetic models may be useful, because defunctionalization and upgrading are important roles of catalytic reactor systems. Second-stage conversions of the oil and asphaltene components were typically low (relative to preasphaltenes conversions), and in many cases were close to zero. These results are consistent with the conventional wisdom regarding thermal/catalytic processing, in which solubilization and upgrading take place primarily in different stages, but appear to apply as well to catalytic/catalytic operation. Trends in resid component conversions in two catalytic/catalytic runs with the same feed coal (Runs 257 and 261) were very similar, in spite of a difference in temperature configuration (high/low vs. low/high). Catalytic/thermal operation in the last part of Run 260 seemed to balance the load in each reactor and result in a near-equilibrium situation with respect to resid conversion (little net conversion or gain of most resid components in either reactor). This situation was not typical of the other runs investigated (Runs 257-262).

Second-stage resid + IOM conversion activities in Run 258 material balance periods decreased significantly with catalyst age, indicating catalyst deactivation. The thermal first stage conversion activity showed no dependence on second-stage catalyst age.

The concentration of 850 x 1050°F material in the recycle oil seems to be influenced primarily by reactor volume in use, perhaps by changing the reactor dynamics (such as the relative thermal and catalytic reaction volumes). During Run 262, the 850°F+ conversion relative to 1050°F+ conversion was quite low in each stage, possibly due to the presence of paraffinic components not easily converted to final products.

RECOMMENDED FUTURE WORK

The resid conversion chemistry of Wilsonville runs prior to Run 257 should be explored in more detail and more-detailed analysis of runs after 257 may also be warranted. Calculation of kinetic rate constants and conversion activities for individual components (instead of only the resid + IOM) might also be of interest. Addition of one more analysis would make it possible to obtain conversions of various hydrogen (proton) types, perhaps providing additional information on the nature of the converted resid.

What more is needed in the future? Innovative kinetic modeling is needed, even for empirical yield and conversion data. For example, experience indicates that bituminous coal converts readily to soluble resid, but less readily to distillate. Conversion of subbituminous coal to solubles is more difficult, but the solubles are readily converted to distillate. An adequate model of liquefaction phenomena would have to account for differences in the coal and resid conversion kinetics in various coals. A comprehensive kinetic model (of proper reaction order) should include the following (preferably mathematically separable) terms: coal (separate terms for IOM and resid reactivity), catalyst (activity and deactivation susceptibility by various routes), and processing conditions (temperature, space velocity, resid concentration, coal and ash recycle concentration, etc.). Current models do not adequately separate processing condition effects from those of the coal and catalyst.

ACKNOWLEDGEMENT

This work was supported by the U. S. Dept. of Energy under contract DE-AC22-89PC89883.

REFERENCES

1. Brandes, S. D.; Robbins, G. A.; Winschel, R. A.; Burke, F. P. "Coal Liquefaction Process Streams Characterization and Evaluation, Analytical Needs Assessment Topical Report", DOE/PC 89883-18, March 1991.
2. Burke, F. P.; Winschel, R. A.; Robbins, G. A. "Recycle Slurry Oil Characterization Final Report - October 1980 through March 1985", DOE/PC 30027-61, March 1985.
3. Winschel, R. A., Robbins, G. A.; Burke, F. P. "Coal Liquefaction Process Solvent Characterization and Evaluation, Technical Progress Report, July 1 through September 30, 1985", DOE/PC 70018-13, December 1985.
4. Winschel, R. A.; Robbins, G. A.; Burke, F. P. *Fuel* 1986, 65, 526-532.
5. Burke, F. P.; Winschel, R. A.; Robbins, G. A. "Coal Liquefaction Process Solvent Characterization and Evaluation - Final Report", DOE/PC 70018-70, September 1989.
6. Detailed Wilsonville Technical Review Meeting handouts and run reports under U. S. DOE Contract DE-AC22-90PC90033 and others preceding it; also see, for example, papers from recent DOE Liquefaction Contractors' Review Meetings and from recent EPRI Clean Fuels Conferences.
7. Various reports under U. S. DOE Contracts DE-AC22-80PC30027, DE-AC22-84PC70018, and DE-AC22-89PC89883.

Table 1. Conditions Used in Recent Wilsonville Runs

Condition	Wilsonville Run					
	257	258	259	260	261	262
Coal* (MF Ash Content, wt %)	BS 2 (11.3)	SC (5.6), BT (7.3)	Ire. (4.5), Ire. (14.9)	BT (6.2)	BS 2 (11.8)	BT (6.4)
Coal Feed Rate, MF lb/hr	166-531	193-293	230-356	251-352	357-548	242-346
Coal Concentration, MF wt %	30-34	30	30-33	30	29-33	30
Resid in Recycle Solvent, wt %	40-50	40-41	40-51	39-40	33-49	32-41
Solids in Recycle Solvent, wt %	12	20-25	6-13	20-21	11-12	19-20
Reactor Vol., % Stg 1/Stg 2	100/100, 50/50	50/50	50/50	100/75, 75/100	100/100	50/50
Catalyst Configuration	Cat/Cat	Th/Cat	Cat/Cat	Th/Cat, Cat/Th	Cat/Cat	Th/Cat, Th/Th
Temperature Configuration	High/Low	High/Low	High/Low	High/Low, Low/High	Low/High	High/Low
Interstage Separation	No	Yes	Yes	Varied	Yes	Yes
Temp. in Stage 1, °F	760-810	825-865	810-825	775-840	790-810	825
Temp. in Stage 2, °F	760-805	740-790	760-790	775-805	800-825	760-810
Stage 1 Catalyst**	Am 1C	None	Am 1C, Sh 324	None, Sh 324	EXP, Cr 324	None
Replace. Rate, lb/T MF Coal	0-3	-	0-4	0-3	0-3	-
Stage 2 Catalyst**	Am 1C	Sh 324	Am 1C, Sh 324	Sh 324, None	EXP, Cr 324	Cr 324, -
Replace. Rate, lb/T MF Coal	0-3	0-3	0-4	3, -	0-3	3, -
Thermal Stage Space Vel., lb MF Coal/hr/ft ³ , (C=Constant)	-	51C-78C	-	31C-43C	-	64C-92C
Catalytic Space Vel., lb feed/hr/lb cat.	3.7-6.7/ 3.7-7.0	-/3.6-5.7	1.8-6.8/ 1.7-6.5	-/3.1-3.9, 2.8-4.0/-	2.9-6.4/ 2.6-6.0	-/4.7-6.6, -/
Stage 1 Catalyst Age, lb (Resid+Solids)/lb cat.	926-2308	-	895-1918	1415-1497	1324-2812	-
Stage 2 Catalyst Age, lb (Resid+Solids)/lb cat.	727-2314	415-3452	718-2710	1330-1368	1090-2238	1315-1545
Slurry Catalyst and Feed Rate: Fe ₂ O ₃ , wt % MF Coal	0	2	0	2	0	2
Molybden L, Mo ppm of MF Coal	0	0	0	0	0	100-1000

Coals are: Black Thunder and Spring Creek (subbituminous), and Burning Star 2 and Ireland (bituminous).

**Catalysts are: Amocat 1C, Shell 324, Criterion 324, and EXP-AO-60.

Table 2. Comparison of CONSOL and Wilsonville Resid Concentrations in Wilsonville Pasting Solvent (V-131B)

Wilsonville Run	Reactor Volume Used, % (1st/2nd Stage)	Resid in V-131B Pasting Solvent, wt %		Fraction of 1050°F ⁺ in 850°F ⁺ (Wilsonville wt %/CONSOL wt %)
		Wilsonville	Difference (CONSOL-Wilsonville)	
Run 262	50/50	37.2 ±2.9	12.5 ±2.0	0.75 ±0.03
Run 261	100/100	43.3 ±6.7	18.5 ±3.5	0.70 ±0.07
Run 260	100/75 (A-C), 75/100 (D-F)	39.4 ±0.8	15.2 ±3.4	0.72 ±0.05
Run 259	50/50	47.4 ±4.1	13.4 ±1.7	0.78 ±0.02
Run 258	50/50	40.8 ±0.4	7.1 ±1.5	0.85 ±0.03
Run 257	100/100, 50/50	46.0 ±4.8	19.1 ±4.9	0.71 ±0.07
257A-257H	100/100	45.7 ±4.9	21.9 ±1.2	0.67 ±0.03
257I-257K	50/50	46.8 ±5.4	11.7 ±0.4	0.80 ±0.02

Table 3. Catalyst Deactivation Rate Calculation For Wilsonville Run 258

Period	Cat. Age, lb (Resid+Cl)/lb Cat.	First Stage A, 10 ⁷	Second Stage A, 10 ⁷
K	559	1.84	3.75
L	1130	1.36	2.22
M	1314	1.57	2.16
Equilibrated (Avg. B, C, D, E, F, H, I)	2523 ±84	1.81 ±0.43	1.05 ±0.61

First Stage: $\alpha = 0.30 \times 10^{-4}$, $\sigma(\alpha) = 1.17 \times 10^{-4}$, $A' = 1.56 \times 10^7$, $\sigma(A') = 1.18$, $R^2 = 0.03$
 Second Stage: $\alpha = -6.2 \times 10^{-4}$, $\sigma(\alpha) = 0.06 \times 10^{-4}$, $A' = 4.96 \times 10^7$, $\sigma(A') = 1.09$, $R^2 = 0.98$
 Note: Units of A' are lb total feed/hr/lb cat, units of α are lb Cat./lb (Resid + Cl).

SEPARATION AND CHARACTERIZATION OF COAL LIQUIDS FROM WILSONVILLE

S. M. Fatemi, D. C. Cronauer, and R. T. Lagman

Amoco Corporation and Amoco Oil Company
Amoco Research Center, P.O.Box 3011, Naperville, Illinois 60566

Keywords: coal liquefaction, LC separation, ion-exchange, coal characterization

ABSTRACT

Ion-exchange and silica gel adsorption techniques were used to isolate and characterize six distillate cuts from three coal liquids generated at the Advanced Coal Liquefaction Facility in Wilsonville, Alabama. Distillates from Black Thunder subbituminous coal liquids contain much higher levels of acidic components than the distillates of Illinois No. 6 or Pittsburgh No. 8 bituminous coal liquids. Saturate fractions of 450-650 °F distillates of all coal liquids were mainly straight chain aliphatics with some indication of branching. The major components identified in the acid fractions from the Black Thunder coal liquid were methyl, ethyl, propyl, and vinyl substituted phenols, benzaldehydes, and methoxy-benzenes. The major components identified in the base fractions from these liquids were methyl and ethyl substituted quinolines, benzene substituted quinolines and carbazoles, methyl-acridines, methyl substituted phenanthrolines and anthracenecarbonitriles. The major aromatic components of the aromatic fractions from Black Thunder coal liquid were methyl, ethyl, and vinyl substituted benzenes and naphthalenes, methyl-anthracene, methyl and ethyl substituted phenanthrene, fluoranthene, pyrene and chrysene.

INTRODUCTION

A typical coal liquid mixture contains a wide range of compound types including acidic, basic, neutral, and various hydrocarbons. The objective of this investigation was to fractionate distillates from coal liquids of varying rank, characterize the fractions and identify the major components of the fractions. Six distillate cuts of three coal liquids from the Advanced Coal Liquefaction Facility in Wilsonville, Alabama, were selected. The samples were 450-650 °F and 650+ °F distillates of coal liquids from Black Thunder subbituminous and Illinois and Pittsburgh seam bituminous coals. The yields of these fractions as a percentage of MAF feed coal are given in Table I.

EXPERIMENTAL

Samples were separated into acid, base, and neutral (ABN) fractions using a non-aqueous ion-exchange separation technique in which a sample dissolved in cyclohexane is passed through two consecutive ion-exchange LC columns. The first was packed with anion resin and the second with cation resin. The material which is not retained by either column was the neutral fraction. Acids were extracted using formic acid in toluene and bases using propylamine in toluene. The fractions were then filtered and stripped of solvent. The neutral fractions were separated into saturate and aromatic (Sat/Ar) fractions using an activated silica gel column. The saturates were eluted from the column with cyclohexane. The retained aromatics were eluted using a mixture of methanol, diethylether, and toluene.

Proton (¹H) NMR spectrometry was used to study the molecular structure of saturate and aromatic fractions. FT-IR spectroscopy was used to study the functional groups in the acid, base, saturate and aromatic fractions from distillates of Black Thunder coal liquid. Thermogravimetric analysis (TGA) in combination with FT-IR was used to determine the decomposition of neutral fractions from 450-650 °F cuts. A gas chromatograph/mass spectrometer (GC/MS) unit was used for detailed characterization and component type identification of acid, base, neutral, saturate and aromatic fractions from distillates of Black Thunder coal liquid.

RESULTS AND DISCUSSION

Separation Data - Recoveries from acid, base, and neutral (ABN) separation cuts are shown in Table II. The ABN recoveries of the 650+ °F cuts of the Illinois and Pittsburgh coal liquids were reasonable and were within the expected ranges. However, that of the neutral fraction from the lower boiling distillate (450-650 °F) was low, possibly due to the loss of light components of the neutral fraction.

Recoveries from the separation of the neutral fractions into saturate and aromatic fractions are shown in Table II. While the saturates and aromatics of the lower boiling distillates (450-650 °F) were clear and thin brownish liquids, respectively, the saturate and aromatic fractions from the higher boiling distillates (650+ °F) were opaque solids and thick brownish liquids. The total recoveries for higher boiling distillates were reasonable, but the total recoveries for the lower boiling distillates were low. Significant amounts of light components were lost from the aromatic fractions of 450-650 °F cuts.

Elemental Analyses Data - Elemental analyses and calculated H/C ratio are given in Table III. The atomic H/C ratio is highest for the saturate fractions, intermediate for the acid, base, and neutral fractions and lowest for the aromatic fractions. The acid fractions have the highest oxygen and the base fractions have the highest nitrogen content. Neither fraction is free of other heteroatoms. In general, the lower boiling cuts had higher oxygen contents than the higher boiling cuts.

NMR Spectrometry Data - The proton NMR data of the saturate and aromatic fractions of both cuts from Black Thunder coal liquid are shown in Table IV. The saturate fractions of 450-650 °F cuts were mainly straight chain aliphatics with some branching. The aromatic, olefinic, and alpha proton values shown for the saturate fractions of light distillates are negligible. While the aromatic fraction of the 450-650 °F distillate exhibits aromatic compounds with highly branched aliphatics attached to the ring(s), the aromatic fraction of the 650+ °F distillate exhibits aromatics with mostly linear aliphatics. Some methyl substituted aromatics were also present in this fraction.

FTIR Spectroscopy Data - FTIR spectra were obtained for the acid, base, saturate and aromatic fractions of both distillates from Black Thunder coal liquid. Spectra of the acid and base fractions of the 650+ °F cut are shown in Figure 1. The main difference between the FTIR spectra of the acids and bases is the presence of a broad band in the 3600-3100 cm^{-1} region of the spectra of the acids. The broad band in this region is assigned to the absorption of O-H and/or N-H groups associated with the intermolecular hydrogen bonding in phenolic, hydroxyl and pyrolytic type compounds. The aromatic C-H stretches are evident from the peaks in the 3050-3000 cm^{-1} and 900-680 cm^{-1} regions of the acid fractions. The peak assigned to the aromatic C=C stretch at 1600 cm^{-1} is also present in the spectra of the acid fraction. Alkanes, both $-\text{CH}_2-$ and $-\text{CH}_3$ groups, are also evident in the 2960-2850 cm^{-1} region of the spectra of the acids. Carbonyl bands (1710-1700 cm^{-1}) can be assigned to the carboxylic acid functional group (COOH). Comparison of spectra of the acid fractions of the 450-650 °F and 650+ °F cuts suggests that; 1. the intensities for the bands assigned to the aromatic ring substitutions (900-680 cm^{-1}) are much lower for the acid fraction from 450-650 °F cut, 2. the aromatic to alkane ratio is higher for the acid fraction of high boiling cut, and 3. the methyl functionalities are slightly higher in the acid fraction from 650+ °F distillate.

The aromatics were still evident in the FTIR spectra of the base fractions, but at a much lower concentration. The presence of the carbonyl peak at 1727 cm^{-1} and the pattern of the bands in the aromatic ring substitution region (900-680 cm^{-1}) suggest the presence of 1,2-disubstituted ester compounds. Alkanes ($-\text{CH}_2-$ and $-\text{CH}_3$) were also evident. The spectra patterns for the two base fractions were nearly identical. The only differences between the spectra of the two bases from the two cuts were the higher ester to alkane and aromatic ratios for the 650+ °F cut.

TGA-FTIR Analyses Data - Stack plots of selected bands from TGA-FTIR analyses of 450-650 °F Black Thunder neutrals are shown in Figure 2. At a TGA temperature up to 300 °F, the neutrals from the Illinois and Pittsburgh coals show very little loss of functional groups. However, the neutral from the Black Thunder coal liquid indicates significant losses of -CH₂- and -CH₃ functional groups at about 150 °F. There are significant losses of aliphatic, aromatic, phenolic and C-H stretch functional groups from all three neutrals at temperatures above 300 °F.

GC/MS Analyses Data - GC/MS chromatograms were obtained for the acid, base, neutral, saturate and aromatic fractions of both distillates from Black Thunder coal liquid. Only selected major components were identified. While there are some similar components in both acid fractions from the high and low boiling cuts (i.e. methyl, ethyl, and propyl-phenols), substituted pyrene and fluoranthene are only present in the acid fraction from the 650+ °F cuts. The major components identified in both acid fractions were methyl, ethyl, propyl, and vinyl substituted phenols, benzaldehydes, and methoxy-benzenes. Methyl substituted carbazoles were also seen in both acid fractions.

The major components identified in the base fraction of 450-650 °F cut were methyl and ethyl substituted quinolines. 2,4-Dimethyl-benzaldehyde, which was identified in both acid fractions, was also identified in the two base fractions. 3-propyl-phenol and anthracene were seen in both the acid and base fractions of 450-650 °F distillates, and components such as pyrene and fluoranthene were seen in the acid and base fractions of 650+ °F distillate. The base fraction of the 450-650 °F cut contained benzene substituted quinolines and methyl substituted acridines, and the base fraction of the 650+ °F cut were methyl substituted phenanthrolines, anthracenecarbonitriles, and benzene substituted carbazoles.

The saturates of both distillate cuts were mostly straight chain alkane with limited branching. Some components with functional groups such as hydroxylamine and alcohols were also identified. The major components of the aromatic fraction of the 450-650 °F cut were methyl, ethyl, and vinyl substituted benzenes and naphthalenes. Those in the aromatic fractions of the 650+ °F cut were methyl and ethyl substituted phenanthrene, fluoranthene, pyrene and chrysene.

CONCLUSIONS

The first step in the analysis of coal-derived liquids is the separation of coal liquid into fractions. Distillates from Black Thunder subbituminous coal contain much higher levels of acidic components than those derived from the bituminous coals. The saturate fractions of all coal liquids were mainly straight chain aliphatics with some branching. The aromatic fraction of the low boiling cut derived from Black Thunder coal liquid contained highly branched aliphatics attached to the rings. However, that of the high boiling cut contained both branched and linear aliphatics attached to the rings. The acid fractions of the distillates derived from Black Thunder coal liquid were methyl, ethyl, propyl, and vinyl substituted phenols, benzaldehydes, methoxy-benzenes, methyl substituted carbazoles, and substituted anthracenes, pyrenes and fluoranthenes. The base fractions of the distillates derived from Black Thunder coal liquid were methyl and ethyl substituted quinolines, benzene substituted quinolines, methyl substituted acridines, methyl substituted phenanthrolines, anthracenecarbonitriles, and benzene substituted carbazoles. The aromatic fractions of these distillates contained methyl, ethyl, and vinyl substituted benzenes, naphthalenes, and anthracene, phenanthrene, fluoranthene, pyrene and chrysene.

ACKNOWLEDGMENTS

We acknowledge K. R. Smith of Mattson Instrument and R. E. Lumpkin of the Amoco Alternative Feedstock Development (AFD) Program for their support.

Table I

Yield of Distillate Cuts (Wt.%, MAF Feed Coal) from Coal-Derived Liquids of Illinois No. 6, Pittsburgh No. 8 and Black Thunder

<u>Feed Coal</u>	<u>Fraction</u>	<u>Yield</u>
Black Thunder	450-650 °F	60
	650+°F	2
Illinois No. 6	450-650 °F	40
	650+°F	31
Pittsburgh No. 8	450-650 °F	44
	650+°F	20

Table II

Recoveries (Wt.%) from Acid, Base, Neutral, Saturate and Aromatic Separations of Distillate Cuts from Illinois No. 6, Pittsburgh No. 8 and Black Thunder

<u>Coal Liquid Cut</u>	<u>Acid</u>	<u>Base</u>	<u>Neutral</u>	<u>Total Recovery</u>
B.T. (450-650 °F)	13.30	3.27	70.10	87.30
Ill. No. 6 (450-650 °F)	3.24	4.18	73.60	81.10
Pitt. No. 8 (450-650 °F)	4.66	3.06	90.60	98.30
B.T. (650+ °F)	17.80	5.42	75.40	98.60
Ill. No. 6 (650+ °F)	3.51	2.95	86.20	92.60
Pitt. No. 8 (650+ °F)	7.32	3.74	90.40	101.50
	<u>Saturate</u>	<u>Aromatic</u>	<u>Total Recovery</u>	
B.T. (450-650 °F)	25.2	63.3	88.5	
Ill. No. 6 (450-650 °F)	23.8	38.6	62.4	
Pitt. No. 8 (450-650 °F)	26.8	45.3	72.1	
B.T. (650+ °F)	19.8	81.7	101.5	
Ill. No. 6 (650+ °F)	23.4	75.1	98.5	
Pitt. No. 8 (650+ °F)	26.2	73.4	99.6	

Table III

Elemental Analyses (Wt. %) of Acid, Base, Neutral, Saturate and Aromatic Fractions of Distillates from Illinois No. 6, Pittsburgh No. 8 and Black Thunder

<u>Fractions</u>	<u>C</u>	<u>H</u>	<u>N</u>	<u>O</u>	<u>S</u>	<u>H/C</u>
<u>BT (450-650 °F)</u>						
Acid	77.84	8.34	1.71	8.08	0.13	1.28
Base	81.66	8.99	4.43	2.73	0.18	1.31
Neutral	86.55	10.08	< 0.30	-----	0.12	1.39
Saturate	84.39	13.13	< 0.30	-----	870 (ppm)	1.85
Aromatic	88.31	9.25	< 0.30	-----	639 (ppm)	1.25
<u>Ill.#6 (450-650 °F)</u>						
Acid	78.41	8.60	1.57	9.47	0.47	1.31
Base	80.16	9.30	3.80	3.64	0.18	1.38
Neutral	87.99	11.55	< 0.30	-----	427 (ppm)	1.56
Saturate	86.12	12.93	< 0.30	-----	-----	1.79
Aromatic	89.09	9.73	< 0.30	-----	568 (ppm)	1.30
<u>Pitt.#8 (450-650 °F)</u>						
Acid	77.78	8.61	0.72	10.15	0.32	1.32
Base	78.50	9.60	2.04	8.89	0.38	1.46
Neutral	88.45	11.63	< 0.3	-----	371 (ppm)	1.57
Saturate	85.47	11.13	< 0.3	-----	-----	1.55
Aromatic	88.69	9.85	< 0.3	-----	385 (ppm)	1.32
<u>BT (650+ °F)</u>						
Acid	81.47	7.67	1.25	7.74	772 (ppm)	1.12
Base	84.62	8.20	4.10	1.79	0.36	1.15
Neutral	89.52	9.52	< 0.3	-----	399 (ppm)	1.27
Saturate	83.97	14.01	< 0.3	-----	239 (ppm)	1.99
Aromatic	89.60	8.04	< 0.3	-----	291 (ppm)	1.07
<u>Ill.#6 (650+ °F)</u>						
Acid	82.06	8.44	2.11	5.82	0.29	1.23
Base	83.83	8.89	3.55	2.09	-----	1.26
Neutral	89.12	9.97	< 0.30	-----	315 (ppm)	1.33
Saturate	86.12	11.83	< 0.30	-----	-----	1.64
Aromatic	90.27	8.88	< 0.30	-----	393 (ppm)	1.17
<u>Pitt.#8 (650+ °F)</u>						
Acid	80.46	8.06	1.00	8.63	0.24	1.19
Base	81.80	8.87	1.70	7.13	0.58	1.29
Neutral	89.50	10.27	< 0.3	-----	219 (ppm)	1.37
Saturate	86.25	11.70	< 0.3	-----	-----	1.62
Aromatic	90.28	9.14	< 0.3	-----	289 (ppm)	1.21

Table IV

Proton NMR Data (atom%) from Saturate and Aromatic Fractions of Distillates from Illinois No. 6, Pittsburgh No. 8 and Black Thunder

Sample	Aromatic	Olefinic	Alpha	Methylene	Methyl
BT (450-650 °F)					
Saturate	0.7	0.8	1.4	69.8	27.4
Aromatic	20.5	0.9	32.9	36.8	8.9
Ill.#6 (450-650 °F)					
Saturate	0.4	0.2	0.6	68.5	30.4
Aromatic	17.2	1.0	33.2	39.3	9.3
Pitt.#8 (450-650 °F)					
Saturate	0.2	0.3	0.9	67.8	30.7
Aromatic	15.6	0.8	32.1	41.4	10.1
BT (650+ °F)					
Saturate	0.3	0.4	0.8	78.0	20.5
Aromatic	29.3	1.2	30.2	32.5	6.9
Ill.#6 (650+ °F)					
Saturate	0.8	0.6	1.7	71.2	25.8
Aromatic	21.5	0.8	30.3	37.9	9.5
Pitt.#8 (650+ °F)					
Saturate	0.3	0.4	1.3	71.7	26.3
Aromatic	20.1	0.8	29.8	39.0	10.3

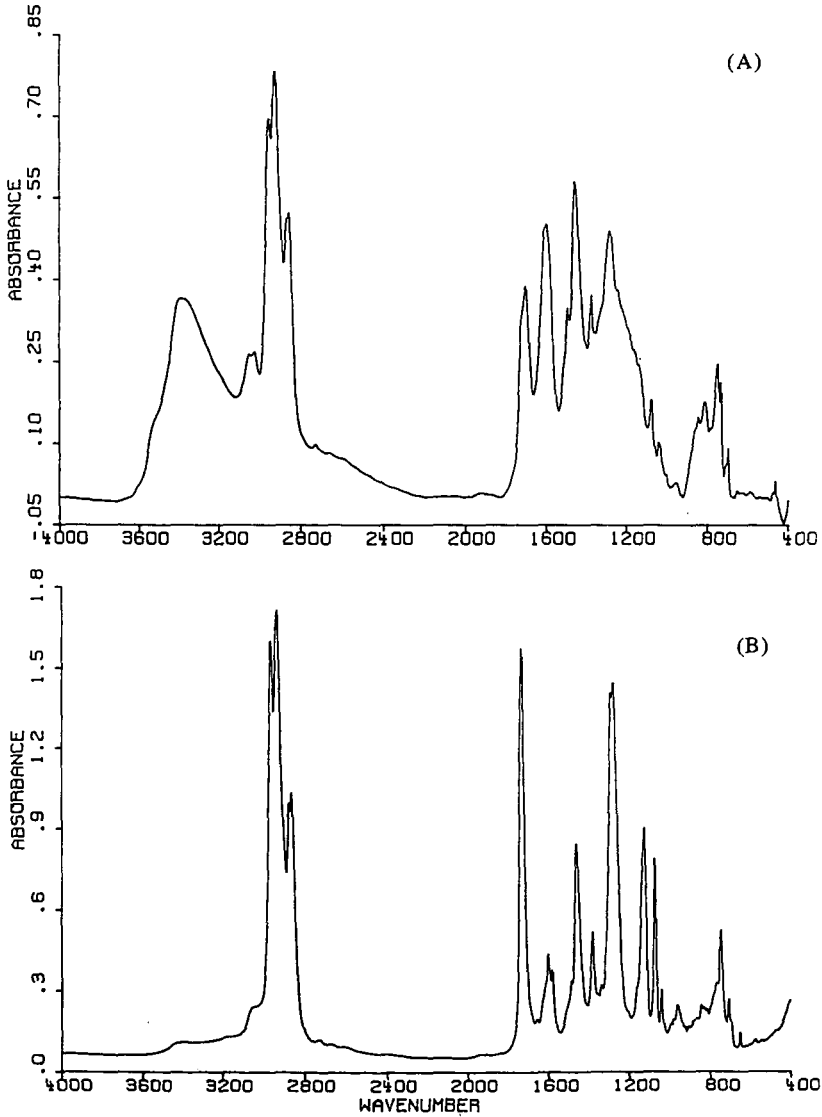


Figure 1. FTIR Spectra of Acid (A) and Base (B) Fractions from 650+ °F Distillate cut of Black Thunder Coal Liquid.

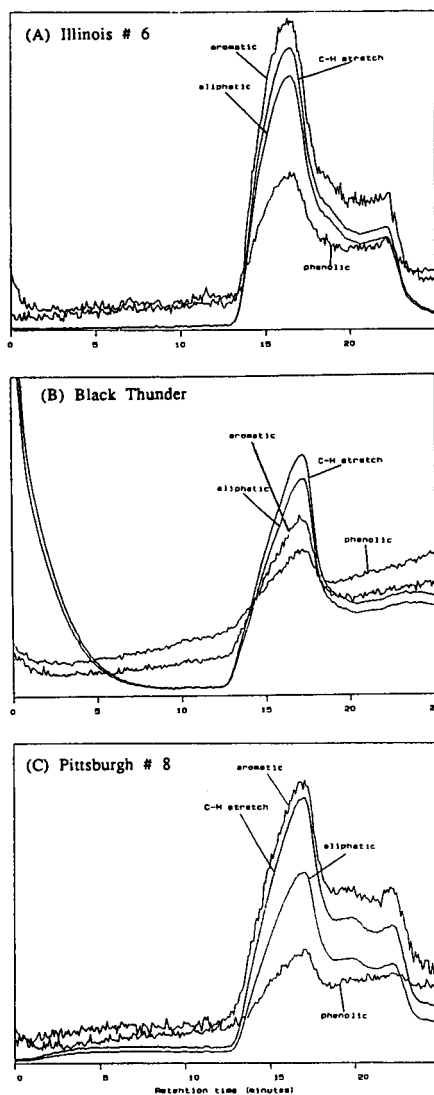


Figure 2. Stack Plots of Selected Bands from TGA-FTIR Spectra of Neutrals from 450-650 °F Distillates of Coal Liquids.

COMPOSITIONAL DIFFERENCES IN NAPHTHA DERIVED FROM NON-CONVENTIONAL FOSSIL FUELS

Robert A. Keogh, Buchang Shi, Shuh-Jeng Liaw,
Arthur Fort and Burtron H. Davis

Center for Applied Energy Research
University of Kentucky
3572 Iron Works Pike
Lexington, KY 40511-8433

Keywords: naphtha, heteroatoms, hydrocarbons

INTRODUCTION

Naphtha derived from non-conventional fossil fuel feedstocks- that is, coal, bitumen, and shale - have the potential to augment the supply of naphtha obtained from petroleum feedstocks. To obtain transportation fuels which meet the current and future environmental regulations, these naphtha will have to be further upgraded. A number of studies suggest that more severe conditions (1-5) are required to obtain suitable heteroatom removal to meet current catalyst requirements both in reforming and hydrotreating.

A number of the studies report on the bulk properties of the naphtha feedstocks and products (elemental analysis, boiling point distributions, etc.). A detailed compositional analysis of the heteroatom and hydrocarbon distribution of the naphtha may offer potential explanations for the severe conditions required and be an important initial step in planning future catalyst formulations for upgrading strategies. These later analyses are not usually reported, at least in significant detail.

EXPERIMENTAL

Samples of naphtha were obtained from the catalytic processing of a western Kentucky tar sand bitumen and for the coprocessing of the bitumen with a Western Kentucky #9 coal in the CAER 1/8 tpd pilot plant. Details of the run and syncrude distillation to obtain the naphtha (IBP-400°F) samples are given elsewhere (6).

Naphtha samples (IBP-380°F) derived from processing an Illinois #6 (bituminous coal) and Black Thunder (subbituminous coal) were obtained from the Wilsonville, Alabama Advanced Integrated Two Stage Liquefaction facility. A light shale oil derived from processing a Cleveland shale (eastern shale) in the CAER Kentort II pilot plant was also included for comparison. Details of the process are given elsewhere (7).

The as-received samples were analyzed by gas chromatography using an HP 5890 series II instrument with a DB-5 column (60m x .32mm; .25 μ m film thickness). Sulfur compounds were analyzed using a Sievers Model 350B chemiluminescence sulfur detector coupled with an HP 5890 Series II gas chromatograph containing a SPB-1 column (30m x .32mm; 4.0 μ m film thickness).

Identification of the hydrocarbons was done by GC/MS and injection of standard compounds. Identification of the nitrogen and sulfur compounds was accomplished by injection of standard compounds. However, the lack of commercially available alkyl

substituted thiophenes and benzothiophenes prevented a number of peaks in the sulfur chromatogram to be identified using this method. From the retention times obtained from the injection of the available standards and current literature (8), it was possible to separate the sulfur chromatogram into classes of sulfur compounds such as thiophenes and benzothiophenes for comparison.

The elemental analyses of the samples are given in Table 1. Carbon, hydrogen, nitrogen and sulfur were obtained using standard methods. Oxygen was determined for the bitumen, coprocessing and coal-derived naphtha by FNAAs. The oxygen content of the shale oil was determined by difference.

RESULTS AND DISCUSSION

A. Hydrocarbon Distribution. The major hydrocarbon classes in the two naphtha samples from Wilsonville are shown in Figure 1. Compounds which are present in greater than .5 wt.% of the total FID chromatogram were identified by GC/MS. The only heteroatom compounds which had a sufficient response in the FID chromatogram are the phenols and these are included in Figure 1 for comparison. Using these guidelines, 65.5 wt.% (Illinois #6 naphtha) and 53.5 wt.% (Black Thunder naphtha) of total areas were identified in the chromatograms.

The major class of hydrocarbons in both coal-derived naphtha samples are cyclohexanes. This class of hydrocarbons includes cyclohexane and one carbon to four carbon substituted cyclohexanes. Methylcyclohexane is the major component in this class for the Illinois #6 derived naphtha. The 2-carbon substituted cyclohexanes are the major components in the Black Thunder derived naphtha. The Illinois #6 naphtha contains higher concentrations of all the cyclohexanes when compared to the Black Thunder naphtha, and this accounts for the overall higher concentration of the cyclohexanes in the Illinois #6 naphtha.

The Illinois #6 naphtha also contains a higher concentration of cyclopentanes than the Black Thunder naphtha. This hydrocarbon class includes cyclopentane and one to three carbon cyclopentanes. The Illinois #6 naphtha contains higher concentrations of all cyclopentanes identified; however, the differences in concentrations of the cyclopentanes in the two naphtha samples are smaller than is observed for the cyclohexanes.

An additional difference in the hydrocarbon distribution is the amount of alkanes, both normal and branched, in these naphtha samples. The Illinois #6 naphtha has significantly more branched and normal alkanes than the Black Thunder naphtha. The normal alkane distributions in both naphtha samples are in the C₄ to C₁₂ range.

The hydrocarbon distribution of the naphtha samples derived from catalytically processing a western Kentucky tar sand bitumen and from the catalytic coprocessing the bitumen with a Western Kentucky #9 coal is shown in Figure 2. The major differences in the compositions between the two naphtha samples are in the yields of normal alkanes and aromatics. Coprocessing the bitumen with the coal produced a naphtha with slightly lower amounts of normal alkanes and aromatics when compared to the naphtha produced from processing the bitumen alone using the same process conditions, catalyst, etc. (6). The carbon number distribution of the normal alkanes ranges from C₆ to C₁₂ in both naphtha samples. The carbon number distributions in the branched alkanes are the same for both

naphtha samples and range from C₇ to C₁₃. The major class of branched alkanes are also the same for both naphtha samples, and are the C₁₀ branched alkanes.

A comparison of the naphtha samples from the coal liquefaction process (Figure 1) and the naphtha samples shown in Figure 2 indicate major differences in the hydrocarbon distributions. The bitumen and coprocessing naphtha samples have a significantly higher amount of alkanes, both normal and branched, and aromatics when compared to the coal liquefaction naphtha samples. Another major difference is in the cycloalkane distributions. The naphtha samples derived during the processing of the bitumen and bitumen plus coal have more alkyl substitutions than the naphtha samples derived from the coal liquefaction process. Five carbon substituted cyclopentanes and cyclohexanes were identified in these two naphtha samples. The coal liquefaction derived naphtha samples have a maximum carbon number of 4 as alkyl substituents.

The hydrocarbon distribution of a distillate sample derived from retorting an eastern shale (Cleveland member) in the Kentort II process (7) is shown in Figure 3. In addition to the hydrocarbons, oxygen and sulfur compounds are in sufficient concentrations to have a response in the FID detector and are included for comparison. The hydrocarbon distribution for processing the shale is distinctly different from the distillates described previously. The major class of hydrocarbons were aromatics (24.4 wt.%), normal alkanes (12.4 wt.5) and olefins (0.3 wt.%). Olefins are only detected in the shale-derived distillate and included a small amount of cyclo-olefins. In addition to the presence of olefins, the major composition difference between the shale derived distillate and the previously described naphtha samples is the low yield of cycloalkanes.

B. Nitrogen Compounds. The nitrogen compound class distributions of this sample set are shown in Figure 4. Identification of the nitrogen compound is made using available standard compounds and the thermionic detector (TSD) as described in the experimental section. The concentrations of the nitrogen compound classes are given in area percent of the total area in the TSD chromatogram.

The major nitrogen class in the Illinois #6 and Black Thunder naphtha samples and the bitumen and coprocessing naphtha samples are the anilines. The anilines include aniline and 1 to 4 carbon alkyl substituted anilines. The 1 carbon substituted anilines are the most abundant compounds in this nitrogen class in the Illinois #6 naphtha. The 2 carbon substituted anilines are the most abundant compounds in this class for the other samples in this study.

The pyridines and quinolines are the next most abundant nitrogen classes of compounds identified in the Illinois #6, Black Thunder, bitumen and coprocessing derived samples. The 1 carbon pyridines are the most abundant compounds in this class in the Illinois #6 and Black Thunder naphtha samples. The 2 carbon substituted pyridines are the compounds with the highest concentration in this class for the bitumen derived naphtha and pyridine is the abundant compound found in this class in the coprocessing derived naphtha.

Quinoline and tetrahydroquinoline have the highest concentrations in this compound class in the Illinois #6, Black Thunder, bitumen and coprocessing samples. One and 2 carbon quinolines were identified in the Black Thunder and Illinois #6 naphtha samples. Substituted quinolines were not detected in the bitumen and coprocessing derived samples.

The distribution of nitrogen compounds in the shale derived distillate are significantly different. The number of compounds represented in the TSD chromatogram are larger than those of the other samples and only 26% of the compounds are identified at this time. The data indicate that the amounts of the pyridine, anilines and quinolines in this distillate are similar. The number of alkyl substitutions are similar to those discussed above.

C. Sulfur Compounds. The sulfur classes of the naphtha samples are shown in Figure 5. The major components identified using the Sievers CSD detector are thiophenes and benzothiophenes. Small concentrations of thiols and sulfides were also identified. The thiophene and benzothiophene classes are characterized by 1 to 3 carbon substitutions and their concentrations depend on their source.

SUMMARY

The hydrocarbon and heteroatom compositions of naphtha samples from non-conventional fossil fuels are reported. This on-going project should provide a well characterized set of samples for future research in hydrotreating and reforming of non-conventional fossil fuels.

ACKNOWLEDGMENT

This work was supported by the DOE contract #De-AC22-90PC90049 and the Commonwealth of Kentucky. The authors also acknowledge the personnel at the Wilsonville liquefaction facility for providing the naphtha samples and for their helpful advice.

REFERENCES

1. L. Xu, R. A. Keogh, C. Huang, R. L. Spicer, D. E. Sparks, S. Lambert, G. A. Thomas, and B. H. Davis, *Prep. - Am. Chem. Soc., Div. Fuel Chem.*, **36 (4)**, 1909 (1991).
2. R. J. Parker, P. Mohammed, and J. Wilson, *Prep. - Am. Chem. Soc., Div. Fuel Chem.*, **33 (1)**, 135 (1988).
3. U. R. Gaeser, R. Holighaus, K. D. Dohms, and J. Langhoff, *Prep. - Am. Chem. Soc., Div. Fuel Chem.*, **33 (1)**, 339 (1988).
4. V. E. Smith, C. Y. Cha, N. W. Merriam, J. Faky, and F. Guffy, Proceedings of the Third Annual Oil Shale, Tar Sand and Mild Gasification Contractors Review Meeting, 166, 1988.
5. H. Frumkin, R. F. Sullivan, and B. E. Strangeland, in "Upgrading Coal Liquids", (R. F. Sullivan, ed.), ACS Symp. Series 156, American Chemical Society, Washington, DC, 1981, pg. 75.
6. R. J. Medina, R. A. Keogh, W. P. Barnett, D. E. Sparks, R. L. Spicer, and B. H. Davis, *Fuel Proc. Tech.*, **27 (2)**, 161 (1991).
7. D. N. Taulbee and S. D. Carter, *Fuel*, **70**, 1245 (1991).
8. B. Chawla and F. J. Di Sanzo, *J. Chromatogr.*, **589 (1-2)**, 271 (1992).

Table 1

Elemental Analysis of Samples

	Wilsonville Samples		CAEFL PIPU Samples		Kentort II Eastern Shale Liquid	
	Bituminous	Subbituminous	Bitumen	Coproprocessing		
C (Wt.%)	86.19	85.34	85.20	84.81	84.58	
H (Wt.%)	13.34	12.25	13.66	13.54	11.84	
N (Wt.%)	.07	.35	.48	.41	.40	
S (Wt.%)	.05	.05	.37	.29	1.79	
O (Wt.%) ¹	.35	2.01	.29	.95	1.39	

¹ Oxygen determined by FNAA for all samples except the shale liquid. This oxygen content was determined by difference.

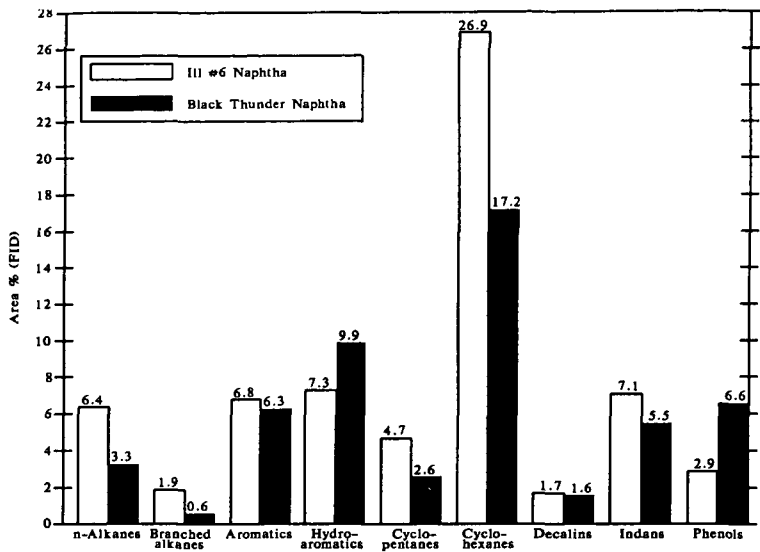


Figure 1. Analysis of Wilsonville naphtha derived from a bituminous and subbituminous coal.

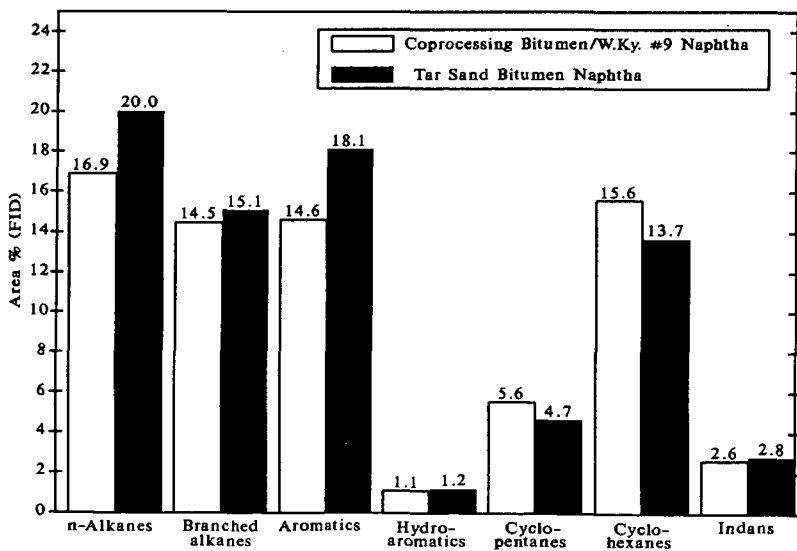


Figure 2. Analysis of naphtha derived from catalytic processing of tar sand bitumen and coprocessing bitumen and a W.Ky. #9 coal.

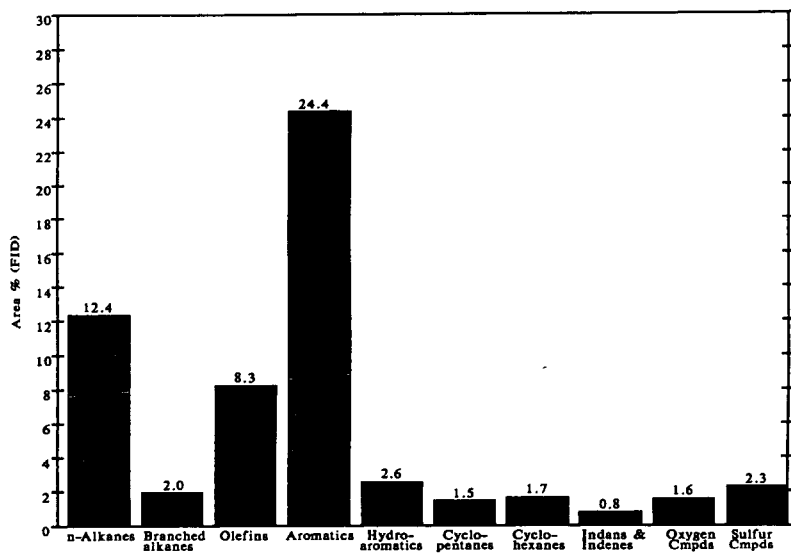


Figure 3. Analysis of a shale derived distillate sample from the Kentort II process.

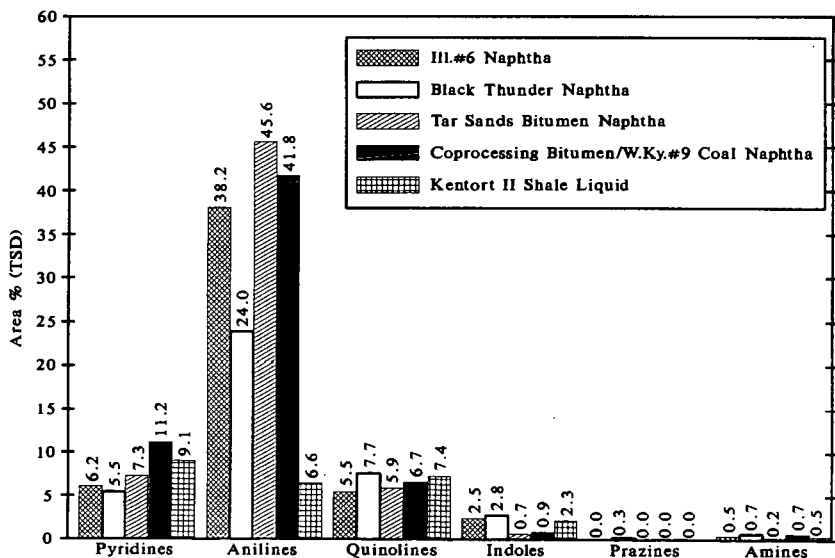


Figure 4. Nitrogen compound class distribution in the sample set.

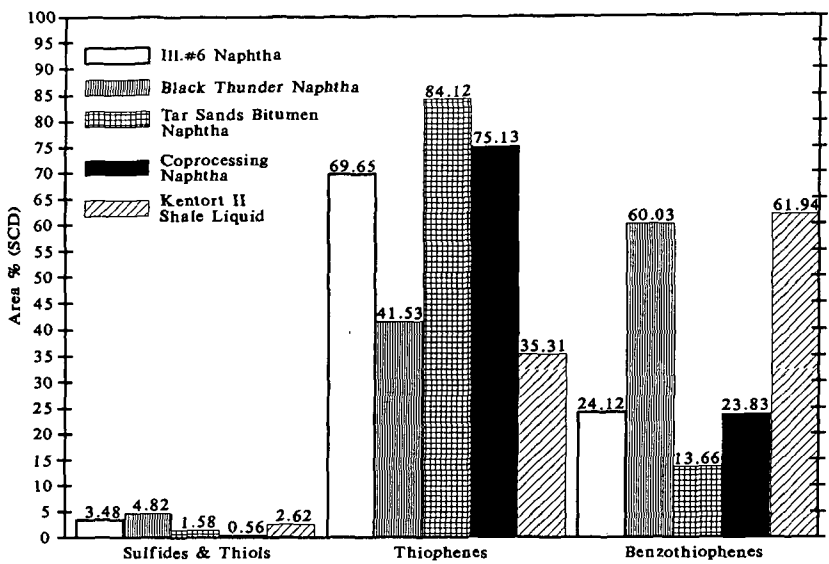


Figure 5. Sulfur compound class distribution in sample set.

ISOBUTENE FROM ISOBUTANOL/METHANOL MIXTURES OVER INORGANIC ACID CATALYSTS

Owen C. Feeley, Marie A. Johansson, Richard G. Herman, and Kamil Klier

Zettlemoyer Center for Surface Studies and
Department of Chemistry, S.G. Mudd #6
Lehigh University, Bethlehem, PA 18015

Keywords: Isobutene, isobutanol, methanol, oxygenates, acid catalysts

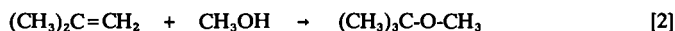
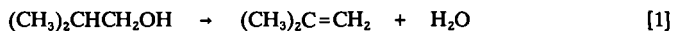
INTRODUCTION

The increasing demand for octane boosting oxygenate compounds, particularly methyl tertiarybutyl ether (MTBE), has led to research efforts investigating alternative sources of these valuable compounds. Currently, MTBE is manufactured from methanol and isobutene *via* a liquid phase synthesis over acid resin catalysts, where isobutene is obtained as a side product from petroleum refinery FCC units (1-3). Although older FCC units can produce 8 wt% C₄ products in their output (4), the typical FCC refinery product slate now contains 1.4 wt% C₄ compounds (5), and improved processes utilizing catalytic additives such as improved ZSM-5 tend to decrease the yield of C₃ and C₄ olefins in the light ends further still (6). Thermal cracking of the isobutane in the light ends can also be carried out to obtain isobutene (5). In any case, the supply of refinery supplied isobutene is limited.

Since MTBE is now the seventh largest produced synthetic organic chemical today (7) and has also been the fastest growing catalytic process during the last decade, a ready supply of both methanol and isobutene is needed. Indeed, it has been predicted that due to continuing and increasing clean air restrictions, the demand for oxygenates (ethers and alcohols) in fuels could increase more than 10-fold by the year 2001 (8). Various alternatives have been sought for increasing the availability of isobutene, and one source of C₄ is butane from natural gas. Although, the butane content in natural gas is low, this source of C₄ is increasingly gaining importance. Among the processes that have been developed for the synthesis of pure isobutene is the endothermic dehydration of tertiary butanol (9).

Another possible source of isobutene for ether synthesis is isobutanol that is produced from synthesis gas. Methanol and isobutanol are the predominant products formed from H₂/CO synthesis gas over alkali promoted Cu/ZnO-based catalysts (10-14). Since the two alcohols are produced together, direct coupling of these two alcohols to produce high octane ethers is also of interest. It has been shown (15,16) that over acid catalysts, the dominant reaction is direct coupling that results in the formation of methyl isobutyl ether (MIBE), a lower octane (17) isomer of MTBE. In addition to ethers, butenes were also observed, and these tended to become more abundant products over inorganic catalysts that were employed at higher temperatures than were the resin catalysts (16).

If a selective catalyst were found for converting isobutanol to isobutene with subsequent reaction with methanol, a desirable route to high octane MTBE from natural gas or coal-derived synthesis gas would be provided, as represented by Equations 1 and 2.



Such a process would alleviate isobutene dependence on petroleum feedstocks. Over the inorganic catalysts previously studied, it was shown that an equimolar mixture of methanol and isobutanol could be directly converted to a methanol/isobutene mixture in high yields with high selectivity using a sulfate-modified zirconia catalyst (16). This catalyst was found to be superior to other solid acid catalysts such as zeolites, silica-alumina and ion exchange resins. The strongly acidic zeolite H-Mordenite, on the contrary, was found to be highly selective for dehydrating the methanol in the mixture to dimethyl ether (DME) (16). No mixed ether was formed and very little dehydration of isobutanol to isobutene was seen. In the present work, the coupling and dehydration reactions were studied over H-ZSM-5 zeolite and γ -alumina. In addition, the pressure dependence of isobutene formation from an isobutanol/methanol mixture was examined over the $\text{ZrO}_2/\text{SO}_4^{2-}$ catalyst.

EXPERIMENTAL

The preparation of the sulfate-modified zirconia ($\text{ZrO}_2/\text{SO}_4^{2-}$) was carried out according to the work of Hino and Arata (17). $\text{ZrOCl}_2 \cdot 8\text{H}_2\text{O}$ was added to aqueous ammonia to precipitate high surface area $\text{Zr}(\text{OH})_4$ that was washed and dried at 100°C overnight. The dried $\text{Zr}(\text{OH})_4$, weighing 10 g was placed on a folded filter paper, and 150 ml of 1 N H_2SO_4 was poured through it. The wet powder was dried at 110°C overnight and then calcined at 620°C for 3 hr. The BET surface area of this catalyst, determined from N_2 adsorption/desorption data, was found to be $60 \text{ m}^2/\text{g}$ and the sulfur content was 0.84% by weight.

The H-ZSM-5 zeolite (Mobil MZ-289) was calcined in air at 400°C for 2 hr prior to loading in the reactor. The Catapal-B was calcined in air at 500°C for 3 hr in order to activate and convert the pseudoboehmite precursor into the γ -alumina phase.

Operating Conditions. The following standard test conditions were used to study the activity and selectivity of H-ZSM-5 zeolite and γ -alumina:

Temperature	90, 125, 150, 175°C (also 200, 225, 250°C for γ -alumina)
Pressure	1 atm (100 kPa)
Methanol feed	1.72 mol/kg catalyst/hr
Isobutanol feed	1.72 mol/kg catalyst/hr
He (+ N_2 trace) flow	16.0 mol/kg catalyst/hr
Catalyst weight	5.0 g

For determining the pressure dependence of the alcohol dehydration reactions and the ether synthesis reactions over the $\text{ZrO}_2/\text{SO}_4^{2-}$ catalyst, the gas composition was maintained while the total reaction pressure was sequentially increased. The following reaction conditions were used:

Temperature	157°C
Pressure (total)	1-62 atm (0.1-63 MPa)
Methanol feed	42.2 mol/kg catalyst/hr
Isobutanol feed	21.1 mol/kg catalyst/hr
He (+ N ₂ trace) flow	756 mol/kg catalyst/hr
Catalyst weight	2.0 g

RESULTS AND DISCUSSION

Reactions of Methanol/Isobutanol Over H-ZSM-5 Zeolite. The space time yields of the major products obtained over H-ZSM-5 zeolite and γ -alumina from methanol/isobutanol = 1/1 reactants at 1 atm with He(N₂) carrier gas are given in Table 1 for a range of temperatures beginning at 90°C, along with those of two of the other inorganic catalysts, H-mordenite and $\text{ZrO}_2/\text{SO}_4^{2-}$, originally reported in previous work (16). The H-ZSM-5 sample was found to be active for isobutanol (i-BuOH) conversion to methylisobutylether (MIBE) and butenes as well as methanol (MeOH) conversion to dimethylether (DME). Of special note is that as the temperature was increased from 125°C to 175°C, the yield of MIBE decreased while the yield of butenes significantly increased. The activation and conversion of i-BuOH over this zeolite catalyst contrasts sharply with that of the H-mordenite studied previously. The H-mordenite sample had been found to be inactive for mixed ether formation from the methanol and isobutanol mixture over the temperature range studied, as shown in Table 1. DME was formed highly selectively and in high yield with only slight conversion of isobutanol, and this was explained in terms of "shape selectivity". Although H-ZSM-5 has smaller pores than H-mordenite, $5.3 \times 5.6 \text{ \AA}$ interconnecting $5.1 \times 5.5 \text{ \AA}$ vs $6.5 \times 7.0 \text{ \AA}$, respectively (19), it is very active for mixed ether formation and butene formation. This shows that the high selectivity toward DME formation observed over H-mordenite is not a general feature of acidic zeolites. This rules out sieving as an explanation for the selectivity pattern seen in H-mordenite. The relative accessibility of the reactants to the zeolitic protons at the low temperatures employed (90-175°C) may be a factor. The intersecting channels of the H-ZSM-5 structure may allow transition state geometries or better access of isobutanol to active sites than the straight non-interconnecting channel system of H-mordenite.

Reactions of Methanol/Isobutanol Over γ -Alumina. The γ -alumina was rather inactive for the conversion of the methanol/isobutanol = 1/1 reactant mixture at the lower reaction temperatures where the other inorganic catalysts were active, and, therefore, higher temperatures (200, 225, and 250°C) were utilized. As seen in Table 1, the selectivity of γ -alumina was unique among the catalysts. The ethers MIBE and DME were selectively formed between 125 and 175°C, while at higher temperatures isobutene formation became more significant. Although not indicated in Table 1, small quantities of iso-octene were also

produced. It is notable that the only butene formed over this γ -alumina was isobutene, whereas for all of the other catalysts under reaction conditions that produce isobutene, significant amounts of the linear butenes, mostly *cis*- and *trans*-2-butene, were also produced. The molar fraction of linear butenes to all butenes formed over the inorganic catalysts, excluding γ -alumina, was generally about one third at 150 to 175°C. The quantities of linear butenes observed were below those calculated for thermodynamic equilibrium. Figure 1 shows the equilibrium constant ratios, i.e. ratio of each linear butene to isobutene, as a function of temperature. The selectivity of isobutanol dehydration over γ -alumina has been studied by several workers (20,21), and it was found that isobutene was formed with over 95% selectivity. The pronounced selectivity of the γ -alumina may be explained by the absence of strong Brønsted acid sites on the surface of alumina (22). The γ -alumina surface has been shown to contain Lewis acid sites associated with basic sites (22). It has been proposed that the acidic and basic sites act concertedly to remove, respectively, the OH⁻ from the alcoholic carbon and an H⁺ from the neighboring tertiary carbon of isobutanol. The presence of strong Brønsted acid sites in the other catalysts, both organic and inorganic, has been associated with carbenium ion chemistry, which leads to rearranged products in isobutanol dehydration (23). Thus, the absence of strong Brønsted acidity in γ -alumina may explain the absence of linear butenes in the product.

Pressure Dependence of Ether and Olefin Synthesis Over Sulfated Zirconia. The effect of reactant pressure on the activity and selectivity of the dehydration of a methanol and isobutanol mixture to butenes and ethers was studied. Nunan et al. (15) had previously studied this reaction over the very strongly acidic ion-exchange resin Nafion-H. It was shown that the rate of butene production decreased and the rate of ether production, mostly MIBE and DME, increased with increasing alcohol pressure. Their kinetic studies indicated that over Nafion-H, dehydration of isobutanol to isobutene required two acid sites. As a consequence, at higher pressures isobutanol inhibited its own dehydration. In studying the pressure dependence of these reactions over $\text{ZrO}_2/\text{SO}_4^{2-}$, the reaction conditions chosen in the present study are similar to those of Nunan et al. (15), and conversions were kept well below 10%.

The space time yields of the products of the reaction of methanol and isobutanol over $\text{ZrO}_2/\text{SO}_4^{2-}$ are presented in Figure 2 as a function of alcohol pressure. Isobutene production decreased strongly with increasing pressure and ether production increased somewhat with increasing pressure. These results are similar to those observed with the Nafion-H resin catalyst (15), and this suggests that the same catalytic functions and properties are occurring on $\text{ZrO}_2/\text{SO}_4^{2-}$ as were found for Nafion-H. The effect of pressure was reversible, i.e. when alcohol pressure was decreased to its original value, isobutene production increased and ether production decreased to their original rates. Even with the ratio of methanol to isobutanol of 2/1, it is clear that at low pressures isobutanol is selectively dehydrated to isobutene with little conversion of methanol to DME or MIBE.

It is apparent from Figure 2 that the reaction pressure hardly affected the yields of the ethers but that low pressures were needed to maximize the selective dehydration of isobutanol to isobutene. It is also evident from Figure 1 that low temperatures are needed when pathways exist (*via* carbenium ion chemistry with Brønsted acids) for the formation

of linear butenes in order to minimize the linear butenes and maximize the proportion of isobutene in the product stream.

CONCLUSIONS

A route to the precursors of MTBE, viz. methanol and isobutene, from the products of higher alcohol synthesis from synthesis gas over alkali-promoted Cu/ZnO catalysts, i.e. methanol and isobutanol, can be made in one step *via* selectively dehydrating isobutanol in the alcohol mixture to isobutene over a sulfate modified zirconia, ZrO_2/SO_4^{2-} , catalyst at moderate temperatures and pressures (e.g. selectivity was $\approx 88\%$ at $157^\circ C$ with methanol/isobutanol = 2/1 under the reaction conditions in Figure 2 and 89% at $175^\circ C$ with methanol/isobutanol = 1/1 under the conditions in Table 1). On the other hand, the H-ZSM-5 zeolite displayed a selectivity toward isobutene plus linear butenes of 77% at $175^\circ C$ under the reaction conditions given in Table 1, and the selectivity of γ -alumina toward isobutene, with no detectable linear butenes, was 53% at $250^\circ C$. In contrast, H-mordenite selectively produced DME from the methanol/isobutanol mixture.

ACKNOWLEDGEMENT

This research was supported by the U.S. Department of Energy (PETC) contract DE-AC22-90PC90044.

REFERENCES

1. Chase, J. D. and Galvez, B. B., Hydrocarbon Process., **60**(3), 89 (1981).
2. Chase, J. D., in "*Catalytic Conversions of Synthesis Gas and Alcohols to Chemicals*," ed. by R. G. Herman, Plenum Press, New York, 307 (1984).
3. Hydrocarbon Process., **68**(11), 96 (1989); and Satterfield, C. N., "*Heterogeneous Catalysis in Industrial Practice*," 2nd Ed., McGraw-Hill, Inc., New York, 260 (1991).
4. Haggin, J., Chem. Eng. News, **67**(23), 31 (1989).
5. Monfils, J. L., Barendregt, S., Kapur, S. K., and Woerde, H. M., Hydrocarbon Process., **71**(2), 47 (1992).
6. Krishna, A. S., Hsieh, C. R., English, A. R., Pecoraro, T. A., and Kuehler, C. W., Hydrocarbon Process., **70**(11), 59 (1991).
7. Chem. Eng. News, **70**(15), 17 (1992).
8. Chem. Eng. News, **70**(19), 26 (1992).

9. Abraham, O. C. and Prescott, G. F., Hydrocarbon Process., 71(2), 51 (1992).
10. Klier, K., Herman, R. G., and Young, C.-W., Preprint, Div. Fuel Chem., ACS, 29(5), 273 (1984).
11. Klier, K., Herman, R. G., Nunan, J. G., Smith, K. J., Bogdan, C. E., Young, C.-W., and Santiesteban, J. G., in "*Methane Conversion*," ed. by D. M. Bibby, C. D. Chang, R. F. Howe, and S. Yurchak, Elsevier, Amsterdam, 109 (1988).
12. Nunan, J. G., Bogdan, C. E., Klier, K., Smith, K. J., Young, C.-W., and Herman, R. G., J. Catal., 116, 195 (1989).
13. Nunan, J. G., Herman, R. G., and Klier, K., J. Catal., 116, 222 (1989).
14. Herman, R. G., in "*New Trends in CO Activation*," ed. by L. Guzzi, Elsevier, Amsterdam, 265 (1991).
15. Nunan, J. G., Klier, K., and Herman, R. G., J. Chem. Soc., Chem. Commun., 676 (1985).
16. Klier, K., Herman, R. G., Johansson, M. A., and Feeley, O. C., Preprint, Div. Fuel Chem., ACS, 37(1), 236 (1992).
17. Spindelbaker, C. and Schmidt, A., Erdoel, Erdgas, Kohle, 102, 469 (1986).
18. Hino, M. and Arata, K., J. Chem. Soc., Chem. Commun., 851 (1980).
19. Meier, W. M. and Olson, D. H., "*Atlas of Zeolite Structure Types*," Butterworths & Co. Ltd., Cambridge, 102 (1988).
20. Knozinger, H. and Scheglila, A., J. Catal., 17, 252 (1969).
21. Herling, J. and Pines, H., Chem. & Ind., 984 (1963).
22. Peri, J. B., J. Phys. Chem., 69, 231 (1965).
23. Kotsarenko, S. and Malysheva, L. V., Kinet. Katal., 24, 877 (1983).

**TABLE 1. Yields over Inorganic Catalysts
(mol/kg cat/hr)**

Pressure 1 atm
 Methanol feed 1.72 mol/kg catalyst/hr
 Isobutanol feed 1.72 mol/kg catalyst/hr
 He + N₂ flow 16.0 mol/kg catalyst/hr
 Catalyst weight 5.0 g

	T _{Reaction}	DME	Butenes	MIBE	MTBE	C ₈ ether
H-Mordenite *	90°C	0.060	----	----	----	----
	125°C	0.660	----	----	----	----
	150°C	0.830	0.068	----	----	0.004
ZrO ₂ /SO ₄ ²⁻ *	90°C	----	----	0.003	----	----
	125°C	0.006	0.067	0.020	0.003	0.008
	150°C	0.027	0.696	0.068	0.009	0.017
	175°C	0.103	1.29	0.049	0.007	----
H-ZSM-5	90°C	0.005	0.001	0.012	----	----
	125°C	0.071	0.169	0.350	0.004	0.003
	150°C	0.261	0.339	0.134	0.003	0.003
	175°C	0.185	1.086	0.131	0.005	0.002
γ-Alumina	90°C	----	----	----	----	----
	125°C	0.006	----	0.007	----	----
	150°C	0.035	----	0.038	----	----
	175°C	0.118	0.002	0.160	----	----
	200°C	0.253	0.023	0.450	----	----
	225°C	0.342	0.242	0.831	----	----
	250°C	0.470	1.073	0.493	----	----

* Reference 16.

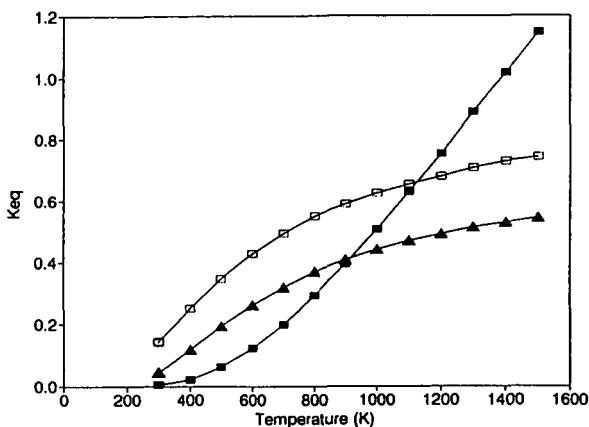


FIGURE 1. The dependence of the calculated equilibrium constants, i.e. mole ratio of linear butenes to isobutene, on the reaction temperature for the conversion of isobutene into 1-butene (■), cis-2-butene (▲), and trans-2-butene (□), beginning at STP conditions.

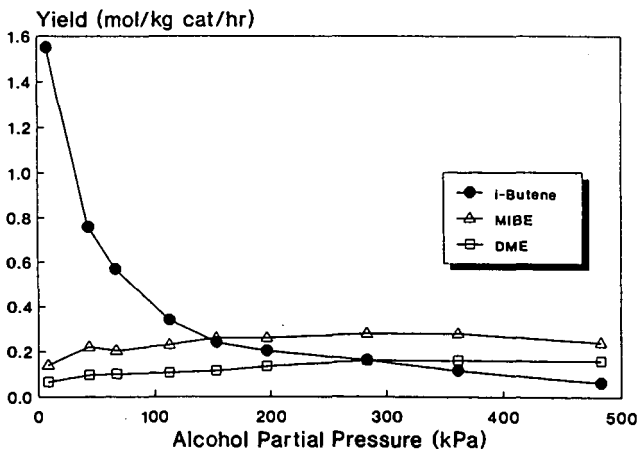


FIGURE 2. Variations of the product yields with the total alcohol partial pressure (methanol/isobutanol = 2/1) over the ZrO_2/SO_4^{2-} catalyst at 157°C. The reaction conditions are described in the Experimental Section.

ACCEPTABILITY OF ALCOHOLS AS GASOLINE SUBSTITUTES

R G Temple and S J Sidhu
Department of Chemical Engineering & Applied Chemistry
Aston University, Birmingham B4 7ET, U.K.

Keywords: Alternative Fuels, Alcohols, Corrosion.

Automobile engines and their fuel systems were developed to use gasoline and their design has been progressively improved for that specific mixture of hydrocarbon fuels. Minor variations in design may render one engine more suitable for "regular" grade (92 RON) fuel while another may be able to use 98 octane fuel to a higher efficiency, but most vehicle owners wish to take advantage of their own preference at the filling station so that one versatile design of engine is required.

The introduction of alcohols (or other oxygenates) presents a range of new properties which may affect engine performance in various ways. Significant differences in volatility, calorific value and latent heat of vapourisation indicate the need for some major adjustments in engine and fuel system dimensions and design for engines which are to use 100% alcohol fuels.

However, there is much to gain by the use of gasohol mixtures since redesign of the internal combustion engine can then proceed by incremental changes rather than a "step change" of unacceptable magnitude. In a large population it is not easy to introduce new fuels unless and in so far as they can be used with minor adjustments only. e.g. to carburettor needle valves or idling controls, etc.

The research described in this paper studied the extent to which alcohols may be substituted without major alterations and especially their acceptability with regard to possible corrosive or deleterious effects on engine and fuel system materials.

Oxidation and corrosion test procedures

Test procedures were designed to simulate actual conditions during engine operation. Small samples of metal or carburettor parts etc., were totally immersed in the test fuel for periods of up to many weeks. While many tests were carried out at ambient temperatures, some higher temperature tests (50°C, 65°C, 90°C) were studied. In all cases periodic aeration of the test fuel reservoir (15 minutes each four hour period) was instigated in order to simulate actual conditions which would obtain in engine operation. Prior to the tests, specimens were ultrasonically cleaned in acetone and similarly cleaned before subsequent weighing and examination.

Corrosion and Oxidation

Corrosion of metals will usually proceed through the formation of an oxide layer on the accessible surface. If this layer is discontinuous as for example in the rusting of iron then corrosion proceeds steadily "eating" into the original material depth. However, if a continuous oxide film results as with some non-ferrous metals then, as oxidation progresses, flakes of oxide layers will detach themselves from the metal surface leaving new accessible surface. In general oxidation follows three courses. Most equations which explain the transient growth at lower temperatures involve logarithmic or exponential terms. They are grouped together as the log laws. At higher temperatures the oxide thickening obeys a parabolic law. This pattern involves a greater risk of flaking or cracking (Fig. 1).

Depending on the temperature and time a metal-oxygen system may follow any one of the above curves. A material which thickens by the parabolic law is accepted as reasonably resistant. However, there is a higher risk of cracking and flaking. If, in contrast the oxidation process follows the log laws then oxidation will almost reach a stand still at a small oxidation thickness. Component designers must therefore seek a material which thickens according to a favourable growth law. Alloying materials can often be found which though not altering the growth law will vary the rate of growth. In some cases the alloying constituent may introduce a new phase at the base of the oxide layer and then the effect of the alloy may give rise to a log law. To some extent the oxidation pattern may then be more predictable. At lower temperatures, as in this work, mechanical separation of the oxide layer may be greatly delayed, at least for a considerable time until a critical thickness is reached. The growth pattern may be altered so that a parabolic thickening at one temperature range may be replaced by rectilinear growth at higher temperatures. Material selection is thus founded on a range of complex ambient influences.

In the case of carburettor components, temperature variation is naturally restricted to liquid phase fuel temperatures and thus growth law prediction is simplified.

Corrosion in engine fuel systems

Corrosion and oxidation rates will be governed by several variables which in engine fuel systems will be dependent on ambient conditions, driving modes, and several design features. Oxidant concentration (in blends) will usually increase corrosion rate. Increased temperatures will also normally increase corrosion rates except where the increased temperature reduces oxygen content of the blend. Acidity (pH value) of the liquid corrodant is a crucial factor determining the likelihood and/or extent of corrosion. Since the oxidation products of alcohols and other oxygenates are carboxylic or other acids, the "strength" of the acid resulting from oxidation is of prime importance. Aeration, resulting in greater access to oxygen, will normally accelerate corrosion/oxidation effects unless the metal or material surface is passive. Flow velocity effects may be significant if corrosion reactions are "diffusion-controlled". Increased velocity will ensure a plentiful supply of fresh ions and will remove corrosion/oxidation products which otherwise would be potentially inhibiting.

In the case of vehicle engines, corrosion/oxidation rates may be of less direct significance than flaking or spalling and consequent weight loss effects. Thus, in this work we placed greater emphasis on any weight loss or gain resulting from corrosion. Samples were treated in significantly lengthy experiments being periodically removed from the test fuel reservoir for weighing. In this way a progressive weight gain and loss profile gave a more or less quantitative indication of corrosion and spalling effects. Figures 2 and 3 are typical of such measurements.

As a further indicator of potential corrosive attack, electrical conductivity of the substitute fuels and of gasohol blends was measured. Methanol (and its blends with gasoline) was shown to be more electrically conductive than ethanol. Some correlation with greater corrosion by methanol was found but other factors contributed significantly, masking this effect.

Vulnerability of metals to alcohols

A longer term study of a greater range of metals and alloys would be needed to identify the most resistant material for use with alcohols in fuel systems. However this work provided some clear indication of which metals might be the most vulnerable in the longer term.

The brasses for example showed greater surface damage in methanol than ethanol but their general resistance to spalling or weight loss indicated that brass components would be satisfactory at elevated temperatures and with aeration. Higher temperature accelerates acid formation in the alcohols giving rise to more severe attack on some metal surfaces. Copper surfaces for instance are highly vulnerable to pitting when in contact with formic acid in methanol. Aluminium is also severely attacked by methanol although the presence of formic acid shows little added effect.

Stainless steel components in methanol (with or without acid) are largely unaffected but this material would be too costly for many components and does not lend itself to simple fabrication techniques as do the "softer" non-ferrous metals copper, zinc, aluminium and their alloys.

Zinc carburettor components showed greater surface damage in methanol than ethanol as judged by the dulling in appearance. This can be related back to the fact that methanol is more electrically conductive than ethanol. However, zinc or zinc-plated components would be much better than aluminium for use with the oxygenates. Copper can be used in the carburettor but care must be taken since this metal can yield large amounts of oxide in the presence of methanol with consequent danger to needle valves and generally inefficient fuel metering.

Conclusions

Our results point the way to material selection for the next generation of carburettors. However, existing materials were not shown to be in imminent danger of corrosive collapse after use of oxygenates. These corrosion studies were carried out in parallel with wide ranging studies of oxygenate fuel performance in a Fiat 127 903cc engine. Visual inspection of the carburettor on this engine after 3-4 years of use with oxygenates and with oxygenate/gasoline blends showing that some pitting of the carburettor had occurred. It is difficult to predict the useful life of carburettor components under these circumstances but this could reasonably be estimated to be several years. It must also be noted that carburettors have until now been largely designed for use with hydrocarbon fuels. As oxygenates begin to feature more prominently as potential alternatives, carburettor design will almost certainly change to use more resistant materials.

Furthermore many of the existing carburettor materials might be retained if some form of inexpensive protective coating were used. These may include polymeric or metallic coating on entire surfaces such as the carburettor body or inlet ducts etc., or on specific vulnerable areas such as the point of a needle valve.

In many countries of the world a finite percentage of alcohol is already used as an extender and to enhance resources of motor fuels. Research studies of this type provide clear indications of where engine designers must seek alternative construction materials for some components.

References

1. Sidhu, J. S., "The Acceptability of Alcohol Fuels for Automobile Engines", Ph.D. Thesis, Aston University, U.K. (1988).
2. Evans, U. R., "The Corrosion and Oxidation of Metals: Scientific principles and practical applications", Edward Arnold Publishers Ltd., London (1976).

Figure 1. Main Types of Growth Laws (2.)

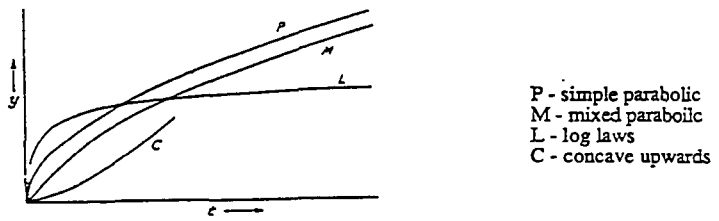


FIG. 2 THE OXIDATION AND CORROSION OF ZINC IN METHANOL/GASOLINE BLENDS AT 50 C

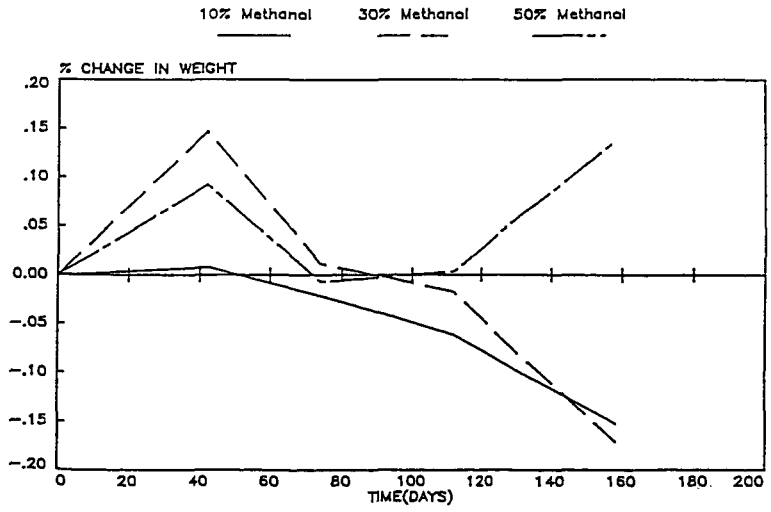
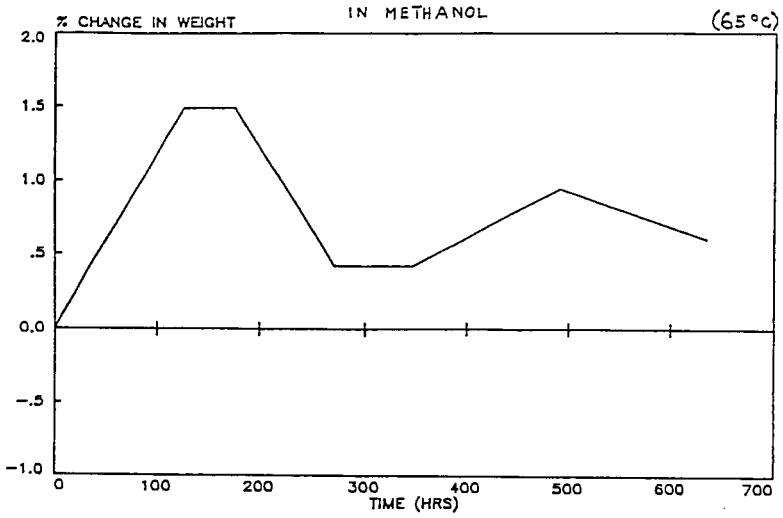


FIG. 3. EFFECT OF TEMPERATURE AND FORMIC ACID ON
OXIDATION AND CORROSION OF ALUMINIUM



ALCOHOLS AND OTHER OXYGENATES AS MOTOR FUELS

R G Temple and N R Gribble
Aston University, Birmingham, UK

Keywords: Alcohols, oxygenates, alternative motor fuels

Alcohols and other low molecular weight oxygenates are known to be potentially valuable gasoline substitutes. While these are generally of interest in relation to the long-term need to secure future motor fuel supplies, there is a more urgent need for substitutes which will improve the octane rating of unleaded fuels. For environmental reasons, oxygenates including alcohols may be preferred to other fuel ingredients which are currently proposed or introduced to replace lead compounds. In addition to octane improvement qualities, oxygenates were assessed with regard to power output and exhaust emissions thus confirming that no great deficiencies in these parameters would be introduced.

TEST PROCEDURES

Oxygenates were studied in a Fiat 127 903 cc engine connected to a Heenan Froude dynamometer to apply a steady variable load. A standard fuel-measuring device and Alcock viscous air flowmeter enabled fuel-air ratios to be closely monitored. Oil, cooling water, and air temperatures etc were continuously monitored to ensure that these remained within the normal range of operational variability. Compression ratios between the four cylinders ranged from 8.92 to 9.13 and this variation was deemed to be acceptable since our concern was to establish the comparative behaviour of these fuels in commercially available engines rather than in single-cylinder studies. The incidence of engine knock was readily detectable at low engine speeds. For routine detection at high engine speeds, a Bruel and Kjaer piezoelectric accelerometer and a CEL piezoelectric pressure washer were installed. The Bruel & Kjaer accelerometer required amplification through a Kistler charge amplifier to give a satisfactory oscilloscope signal, while the "knock" washer gave a satisfactory pressure trace without amplification.

A standard low-leaded base gasoline of the F-7 series was used for comparison and as a base for alcohol and oxygenate blends.

Oxygenates used:

The following alcohols, ethers, esters, and ketones were used in blends containing between 5 and 20% oxygenate in gasoline .

Alcohols	Methanol Ethanol Tert Butanol
Ethers	Methyl tert butyl ether Diiso propyl ether Anisole
Esters	Dimethyl carbonate Methyl acetate
Ketones	3 methyl butan-2-one 4 methyl pentan-2-one Acetone Methyl ethyl ketone

The alcohols and MTBE are well known gasoline substitutes, some having been considered and used over the last sixty years. Other oxygenates in this list were chosen because of their branched structure, small molecular size and, in some cases, prior knowledge of their RON and MON. Current production cost was also important although bulk production and new methods of synthesis could make many other similar oxygenates viable.

The concentrations used in experiments were varied so as to limit total blend oxygen content to a maximum of around 4% by weight. This is within the limits of good drivability ie giving no observed problems caused by the leaning effect due to the extra oxygen in the combustion process.

The experiments aimed to test the various oxygenates with regard to improved octane rating and to test various mixtures of oxygenates combining two or more chemical types and changing individual components to assess whether a synergistic effect is exhibited.

The results obtained for single oxygenates showed several chemicals to have similar effects in similar concentrations provided that their oxygen content was comparable. Dual combinations of oxygenates were all tested as 10% vol/vol blends producing 2-4% wt/wt oxygen in the blends. Treble combinations were blended at 15% vol/vol.

Methanol/MTBE/3 methyl butan-2-one and methanol/MTBE/4 methyl pentan-2-one were seen to be superior while methanol/MTBE/TBA also exhibited good knock "protection". (Figs. 1 and 2)

Comparison of multicomponent blends with the effect of individual components is not always readily seen, since the individual effect of a smaller oxygenate percentage is not always very obvious. Comparing results on the basis of percentage weight of oxygen in the blend showed little significant correlation. Blending octane numbers cited in the literature vary dramatically with notable gaps for some of the ketones.

EXPERIMENTAL RESULTS

Octane Improvement To determine apparent increase in quality due to oxygenate addition several engine runs were performed using the base fuel. Then oxygenate blends showed a clear comparison. Combinations of oxygenates were regarded as most important in order to study synergistic effects especially of mixtures of chemical type and components so as to establish where chemical type was of the greater importance.

The results initially suggested methanol plus MTBE with a ketone was better than average and methanol plus MTBE with TBA was promising. Later results showed dual blends may be equally valuable. For example MTBE and methanol was one of the best combinations while TBA and ketones in the triple blends were valuable in replacing the ether but did not improve the anti knock quality.

CFR tests were carried out and showed that the oxygenates led to a greater RON than MON increase. This is due to the higher sensitivity of the oxygenates compared with the base gasoline. However the replacement of MTBE by 4 methyl pentan-2-one reduced the sensitivity of the blend due to its own very low sensitivity. Small amounts of 4 MP2 imparted no change in RON but a decrease in MON.

Power output A number of blends showed increased power output when oxygenates were present with the greatest increase exhibited at low speeds. This may result in better acceleration performance with maximum power output largely unaffected. Increases of up to 5% were exhibited and in our work a 6:3:2 blend of methanol/MTBE/and 4 MP2 gave some of the best results.

Viability of ketones as blending components

Acetone, MEK and 4 MP2 are among the hundred largest volume production organic chemicals, and some may be close in price to more usually accepted blending components. Their very high octane numbers make them worth further consideration. Tonnage production of such compounds may, however, be dependent on other industrial useage. For example, 4 MP2 is used widely as a solvent and degreasant. Tonnage used as an automobile paint solvent is being reduced in an attempt to reduce evaporative emissions to the atmosphere. Replacement by water-based solvents should release large tonnages of this ketone for fuel blends in the medium term as production plants are left with reduced total demand. Although this reduction may not augur well for future price stability, the medium term availability may provide a period in which the merits of 4 MP2 as an engine fuel ingredient could be well established.

CONCLUSIONS

This work showed that combinations of oxygenates including alcohols, ethers and ketones can be highly advantageous in raising octane ratings by 3 or 4 without modification to engine and fuel system. Lower exhaust emissions are to be expected with more oxygen in the fuel and these and improved power output are additional benefits.

Alcohols and MTBE are used individually by many countries and some, notably Switzerland, include them together in some gasoline blends. Increasing interest is being shown in other ethers (such as dimethyl ether in the USA and elsewhere) and production plants for such fuel components are coming to be seen as potentially viable. The higher cost of ketones such as 4 MP2 has limited the interest in these as gasoline substitutes but current demand changes may release lower cost supplies and a world wide interest, increasing production for automobile fuel use, could well bring massive economies of scale.

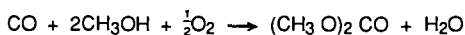
The inexorable moves to unleaded fuels will bring these oxygenates a higher profile as potentially viable gasoline substitutes with major advantages in terms of octane requirement, power output and atmospheric quality.

Clean air legislation in the USA and elsewhere is giving a boost to several of the oxygenates which we have studied. For example, the 1990 US Clean Air Act placed tough restrictions on gasoline blending

while tightening constraints on exhaust emissions. A 25% reduction in high octane aromatic compounds is called for by 1995. New blending ingredients are needed which meet the Act's requirements and replace the lost octane rating. MTBE has been widely recommended for this role⁽²⁾ but Dimethyl ether (DME) may be equally promising.

A new one-step synthesis yields methanol and DME from CO-rich synthesis gas and is expected to show cost advantages over traditional catalytic dehydration of methanol. The DME/methanol product could be used as a transport fuel since the DME gives the methanol an improved cold-start facility. Thus, as a separate synthetic fuel or as an octane improver, DME could compete with MTBE without competing for a C₄ feedstock.

Another oxygenate which has attracted interest as an octane booster is di methyl carbonate (DMC). This compound was synthesised in the 1980's as a replacement for phosgene in carbonylation reactions⁽³⁾. Found to be "environmentally-friendly", DMC is finding other demands in pharmaceuticals and plastics but its greatest potential may be as an octane booster. Again it does not compete with MTBE being synthesised from methanol:



A 12,000 t/y plant is operating in Italy and the feasibility of production in the USA is under consideration with methanol and methane more readily available. As a fuel blending component DMC reduces the amount of ozone emitted by the engines of older vehicles and shows the other cleaner exhaust properties typical of oxygenates.

As the world-wide trend towards unleaded fuels gathers pace, all the oxygenates will gain a higher profile as gasoline substitutes and octane boosters. Relying mainly on synthetic production routes the choice of "best oxygenate" will depend primarily on ease of synthesis to keep costs within reasonable limits.

Synthetic oxygenate mixtures such as the methanol/DME product referred to above could well prove the most viable. As with petroleum fractionation the usefulness of a mixture of compounds (c/f the "gasoline fraction") may well be decisive in settling which formulation will win the "best oxygenate" label.

Apart from compliance with the general constraints on emissions of CO, hydrocarbons, and NOX, there will be increasing concern to combat the "greenhouse effect". Apart from enhancing engine performance efficiency, alcohols, especially ethanol, may hold their place as the most "environmentally-advantageous" automobile fuels. This is especially true if the alcohol can be produced from a short-rotation biomass source such as cane-sugar. Agricultural production of the sugar cane absorbs CO₂. If one then produces ethanol by the well-known fermentation route, the subsequent combustion of the alcohol as motor fuel is merely **recycling** that CO₂ to the earth's atmosphere.

While the choice of feedstock for automobile fuel will remain largely dependent on price, such environmental issues will maintain the interest in the alcohols. In the next decade one may well see a range of fuels based on alcohols making further inroads into the world-wide gasoline demand.

REFERENCES

1. Gribble, N.R. "Alcohols and other Oxygenates as Motor Fuels" Ph.D. Thesis, Aston University, U.K. 1987.
2. Ottewell, S. "One-Step DME clears the Air". The Chemical Engineer, 25 July 1991.
3. Bolton, L. "Enichem synthesis unpacks DMC potential". The Chemical Engineer, 9 April 1992.

ACKNOWLEDGMENT: The authors wish to thank Esso Research, U.K. for a cooperative (CASE) award in support of this research.

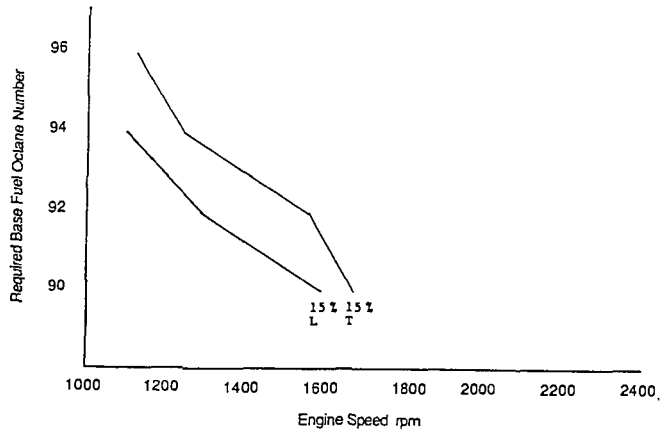


Figure 1 1:1:1 Methanol:MTBE:TBA

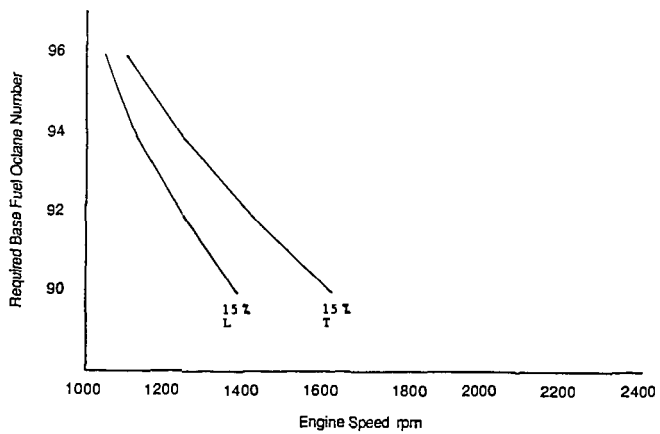


Figure 2 1:1:1 Methanol:MTBE:3MB2

LIQUEFACTION OF HYDROCARBON-RICH MICROALGA

Yutaka Dote, Shigeki Sawayama, and Shinya Yokoyama
National Institute for Resources and Environment
16-3 Onogawa, Tsukuba, Ibaraki 305, Japan

Keywords: liquefaction, Botryococcus braunii, liquid fuel

INTRODUCTION

A colonial green microalga, Botryococcus braunii, accumulates hydrocarbons(terpenoids) 30-70 % of its dry weight by fixing carbon dioxide in the atmosphere (1). Thus, the use of B. braunii could contribute to the reduction of the greenhouse effect if the hydrocarbons could be used as alternative liquid fuel. In laboratory, hydrocarbons of algal cells have been separated by extraction with organic solvent after freeze-drying and sonicating the algal cells. However, these procedures are not suitable for separation on a large scale because these are costly. Therefore, an effective method is expected for separating hydrocarbons as liquid fuel from harvested algal cells with high moisture content. We have proposed a new method for separating liquid fuel from algal cells of B. braunii by direct thermochemical liquefaction. The direct thermochemical liquefaction can convert wet biomass such as wood and sewage sludge to liquid fuel at around 300°C and 10 MPa using catalyst such as sodium carbonate (2,3). At the same time, the liquid oil can be easily separated (4). Therefore, it is expected that an amount of oil more than that of hydrocarbons in algal cells could be obtained because of the liquefaction of organic materials such as fiber, cellulose, and protein other than hydrocarbons in algal cells. In this paper, we discussed the applicability of the liquefaction of algal cells of B. braunii and the yield and properties of the liquid oil obtained by the liquefaction.

EXPERIMENTAL

Botryococcus braunii Kutzing Berkeley strain was used for liquefaction. Culture conditions were as follows: continuous light at 3000 lx and 25°C in a modified Chu 13 medium (5). Algal cells were washed three times by filtration with a nylon sheet of 20 µm mesh. The properties of the algal cells are listed in Table 1. The algal cells contained 92 % of water. Hydrocarbons in algal cells were separated as follows: freeze-dried algal cells were sonicated with 50 ml of hexane for 30 min by a Sonicator 201M(Kubota, Japan). The suspension was filtered through No.2 filter paper(Toyo Roshi, Japan) and the hexane solution was evaporated at 30°C under vacuum conditions.

Liquefaction was performed in a 300ml autoclave made of stainless steel. The wet algal cells(about 30g) were charged in the autoclave. After purging the residual air with nitrogen, nitrogen was added to 2 MPa and then the autoclave was sealed. The reaction was started by heating the autoclave by an electric furnace. After heating the autoclave up to the required temperature(200 and 300°C), the temperature was maintained for 1 h, and then the autoclave was cooled.

The procedure for the separation of products is shown in Fig. 1. The oil obtained by liquefaction was defined as dichloromethane soluble(in this paper referred to as primary oil). Hydrocarbons in primary oil was extracted with hexane(10 ml-hexane/g-dichloromethane soluble x 5).

The analysis of elemental composition(carbon, hydrogen, and nitrogen) was made by a Perkin Elmer Elemental Analyzer(Model 240) and the content of

oxygen was calculated by difference. Heating value(MJ/kg) was calculated according to Dulong's formula, $Q=0.3383C+1.442(H-O/8)$, where C, H, and O are the weight percentage of carbon, hydrogen, and oxygen, respectively. Viscosity was measured by a viscometer(HAAKE, RV12) at 50°C.

RESULTS AND DISCUSSION

Properties of hexane soluble of the raw algal cells. The properties of the hexane soluble of the raw algal cells are shown in Table 2. The hexane soluble was obtained in the high yield of 58 % of its dry weigh, and had the good fluidity(56 cP) and the high heating value(49 MJ/kg).

Primary oil. The properties of primary oil are shown in Table 3. The yield of the primary oil obtained at 300°C were 52.9 % and that at 200°C was 56.5 %; these values were a little lower than the yield of the hexane soluble of the raw algal cells. This suggests that hydrocarbons of the raw algal cells were partly converted to dichloromethane insoluble materials such as char.

The heating value of the primary oil obtained at 300°C was 47.5 MJ/kg and that at 200°C was 42.0 MJ/kg; these values were equivalent to petroleum oil. Especially, the heating value of the primary oil obtained at 300°C was much higher than that of the oil obtained by liquefaction of other biomass. The viscosity of the primary oil obtained at 300°C was as low(94 cP) as that of the hexane soluble of the raw algal cells. However, the viscosity of the primary oil obtained at 200°C was too high to measure it; the primary oil was like a rubber. Therefore, the primary oil obtained at 300°C could be used as fuel oil.

The oxygen content of the primary oil obtained at 300°C was a little higher than that of the hexane soluble of the raw algal cells. However, it was much lower than that of the oil obtained by liquefaction of other biomass.

Hexane soluble. The properties of the hexane soluble of primary oil are shown in Table 4. The yield of the hexane soluble of the primary oil obtained at 300°C was 44 % and that at 200°C was 39 % on a dry algal cells basis. This meant that the primary oil obtained at 300°C contained 83% of hexane soluble and that at 200°C contained 69 % of hexane soluble. The elemental composition of the three hexane solubles was almost equal. The hexane solubles of the primary oil obtained at 300 and 200°C had good fluidity as well as the hexane soluble of the raw algal cells. In spite of thermal treatment at high temperature, the same properties of the hexane soluble of primary oil as that of the hexane soluble of the raw algal cells.

In summary, The direct thermochemical liquefaction could provide an effective method for separating liquid fuel from the hydrocarbon-rich microalga, *B. braunii*. Although the yield of primary oil was a little lower than that of the hexane soluble of the raw algal cells, the yield of primary oil might be possibly improved by use of suitable catalyst such as sodium carbonate. The bench-scale plant to continuously liquefy sewage sludge run successfully (6); thus, it might be possible to liquefy the algal cells on a large scale.

ACKNOWLEDGMENT

The authors thank Professor Katsumi Yamaguchi of The University of Tokyo for graciously providing *Botryococcus braunii* Kutzing Berkeley strain.

References

- 1) K. Yamaguchi, H. Nakano, M. Murakami, S. Konosu, O. Nakayma, M. Kanda, A. Nakamura, and H. Iwamoto, Agric. Biol. Chem. 51, 493-498, 1987

- 2) T. Ogi, S. Yokoyama, T. Minowa, and Y. Dote, *Sekiyu Gakkaishi* 33, 383-389, 1990
- 3) S. Yokoyama, A. Suzuki, M. Murakami, T. Ogi, K. Koguchi, and E. Nakamura, *Fuel* 66, 1150-1155, 1987
- 4) A. Suzuki, T. Nakamura, S. Itoh, and S. Yokoyama, *Kagaku Kogaku Ronbunshu* 15, 326-334, 1991
- 5) C. Largeau, E. Casadevall, C. Berkaloff, and P. Dhameincourt, *Phytochemistry* 19, 1043-1051, 1980
- 6) A. Suzuki, T. Nakamura, S. Itoh, and S. Yokoyama, *Research Journal of Japan Sewage Works Association* 27, 104-112, 1990

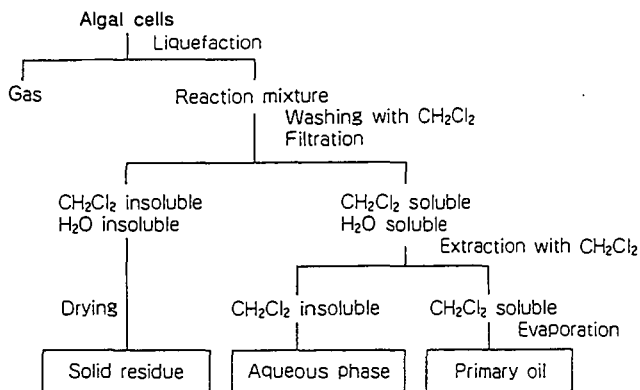


Fig.1 Procedure for the separation of primary oil

Table 1 Properties of microalga used for liquefaction

Moisture content	Dry solid	Ash	Organics
(%)	(%)	(%) ¹⁾	(%) ¹⁾
92.0	8.0	2	98
Elemental analysis (%) ¹⁾			
C	H	N	O
68.7	10.9	1.3	19.1

1) On a dry algal cells basis

Table 2 Properties of the hexane soluble of raw algal cells

Yield (%) ¹⁾	Heating Value (MJ/kg)	Viscosity (cP, @50°C)	Elemental analysis(%)			
			C	H	N	O
58	49.4	56	84.6	14.5	0.1	0.9

1) On a dry algal cells basis

Table 3 Properties of primary oil

Temp. (°C)	Yield (%) ¹⁾	Heating Value (MJ/kg)	Viscosity (cP, @50°C)	Elemental analysis(%)			
				C	H	N	O
300	52.9	47.5	94	83.3	13.7	0.4	2.6
200	56.5	42.0	-	78.6	11.9	0.0	9.5

1) On a dry algal cells basis

Table 4 Properties of the hexane soluble of primary oil

Temp. (°C)	Yield (%) ¹⁾	Heating Value (MJ/kg)	Viscosity (cP, @50°C)	Elemental analysis(%)			
				C	H	N	O
300	44	49.2	77	84.5	14.3	0.1	1.1
200	39	50.3	170	83.5	15.3	0.1	1.1

1) On a dry algal cells basis

**CATALYTIC ACTIVITY OF OXIDIZED (COMBUSTED) OIL SHALE FOR
REMOVAL OF NITROGEN OXIDES WITH AMMONIA AS A
REDUCTANT IN COMBUSTION GAS STREAMS**

John G. Reynolds, Robert W. Taylor, and Clarence J. Morris

University of California
Lawrence Livermore National Laboratory
Livermore, CA 94551

Keywords: Oil Shale, NO_x Removal, Combustion Flue Gas

ABSTRACT

Oxidized oil shale from the combustor in the LLNL hot recycle solids oil shale retorting process has been studied as a catalyst for removing nitrogen oxides from laboratory gas streams using NH₃ as a reductant. Combusted Green River oil shale heated at 10°C/min in an Ar/O₂/NO/NH₃ mixture (~ 93%/6%/2000 ppm/4000 ppm) with a gas residence time of ~ 0.6 sec exhibited NO removal between 250 and 500°C, with maximum removal of 70% at ~ 400°C.

Under isothermal conditions with the same gas mixture, the maximum NO removal was found to be ~ 64%. When CO₂ was added to the gas mixture at ~ 8%, the NO removal dropped to ~ 50%. However, increasing the gas residence time to ~ 1.2 sec, increased NO removal to 63%.

These results are not based on optimized process conditions, but indicate oxidized (combusted) oil shale is an effective catalyst for NO removal from combustion gas streams using NH₃ as the reductant.

INTRODUCTION

Green River oil shale contains 10+ wt % organic material. Pyrolyzed for a few minutes at 500°C, this shale releases ~ 80% of the organic matter as oil vapors and non-condensable gases. The balance of this organic material is left in the retorted shale as a solid (char). Efficient oil shale processes, such as the LLNL hot recycle solids (HRS) retort process, burn this char to heat the raw feed shale (1).

The ratio of nitrogen to organic carbon in Colorado Oil shale and retorted shale is higher than in most other fossil fuels. As a result, the concentration of NO_x and NH₃ in the combustion flue gas of the HRS process are high. Under normal HRS pilot plant operations, the combustion flue gas contains ~ 5% O₂, ~ 50 ppm NH₃, and ~ 500 ppm NO. This NO emission level is high by a factor of ~ two for current coal combustion standards in the U. S. (2). Under oxygen starved (fuel rich) combustion, the concentration of NO falls to ~ 250 ppm.

At present, a practical way of lowering NO_x emissions in industrial boilers employs selective catalytic reduction (SCR) using NH₃ at ~ 300°C (3). Non catalytic reduction of NO_x by NH₃ at about 950°C (thermal denox) is also practiced (4).

We are investigating factors which influence emissions of NH_3 and NO during oxidation of retorted shale. We have reported on the oxidation and thermal decomposition of NH_3 , as well as utilizing retorted oil shale for NO reduction (5). Here we report the use of NH_3 as a reducing agent for NO over oxidized (combusted) oil shale.

EXPERIMENTAL

Experiments were performed at constant heating rates or isothermally at ambient-pressure in a 2.5-cm diameter, 50-cm long silica glass tube mounted vertically in an electric furnace. The thermal center of the tube was filled over a length of ~ 8 cm with the material being examined. Bed materials were either oxidized (combusted) Green River oil shale (22 gal/ton) or porous white firebrick. The shale bed used in the constant heating rate experiments was prepared by burning shale at temperatures as high as 850°C in air which assured that a significant fraction of the calcite (CaCO_3) in the shale was decomposed to lime (CaO), and no organic carbon remained. The shale used in the isothermal experiments was taken from the HRS pilot plant where combustion was at temperatures below 750°C , resulting in little CaCO_3 decomposition. This shale sample contained ~ 0.3 wt % unburnt char, typical of processed shale. Both shale samples weighed 27 g and had a particle size range from 1.4 to 2.8 mm. The bed porosity was $\sim 40\%$, and the porosity of the individual shale grains was $\sim 25\%$.

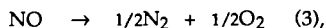
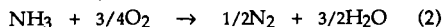
Temperature of the bed was measured with a thermocouple located at the center of the bed. The gas mixtures were passed down flow at a rate of either ~ 1 or ~ 0.5 L/min. At the 1 L/min rate, the transit or contact time between the flowing gas and shale at 300°C was about 0.6 sec. The gas compositions were constructed to simulate an idealized HRS combustor output, with and without CO_2 . Ar was selected as the carrier gas to facilitate detection of product N_2 .

Analysis of NH_3 , NO , NO_2 , N_2 , H_2 , O_2 , H_2O , and Ar was by an EXTREL Questor model mass spectrometer. Calibration for all gases except H_2O was accomplished by means of commercial gas standards and air. The mass spectrometer was connected to the reactor by a 304 SS line heated at 150°C . Data was taken every 10 to 15 sec. Because both N_2O and CO_2 have m/z 44, they can not be differentiated in the mass spectrometer. In the cases where CO_2 was absent in the inlet gas, m/z 44 was considered due mainly to N_2O . In the initial experiments at constant heating rates, the N_2O was also measured by a BIO-RAD FTS 40 FTIR. In the cases of CO_2 in the inlet gas, m/z 44 was assumed to be all CO_2 , and no N_2O measurements were made. In all cases, m/z 28 was corrected for CO fragmentation from CO_2 . No NO_2 was observed.

Whenever NH_3 and O_2 were passed into the mass spectrometer, H_2O and N_2 were observed as products. The ratio of H_2O to N_2 corresponded to NH_3 combustion. Approximately 20% of the NH_3 was burnt in the hot MS source. This side reaction was accounted for by measuring a baseline concentrations of these species before each run.

RESULTS AND DISCUSSION

Nitrogen oxide removal utilizing SCR with NH_3 as the reductant is chemistry which could go through several reactive oxide intermediates, such as N_2O , NO_2 , N_2O_4 , N_2O_3 (6). In this initial study, we make no attempt to study the mechanism(s) of the reactions. We only use the stoichiometry of suspected reactions to substantiate (but not necessarily prove) the overall global reactions. The general global reactions which need to be considered are:



where reaction (1) is a combination of reactions (2) and (3). Potential competing reactions which may be observed under the conditions of these experiments are:

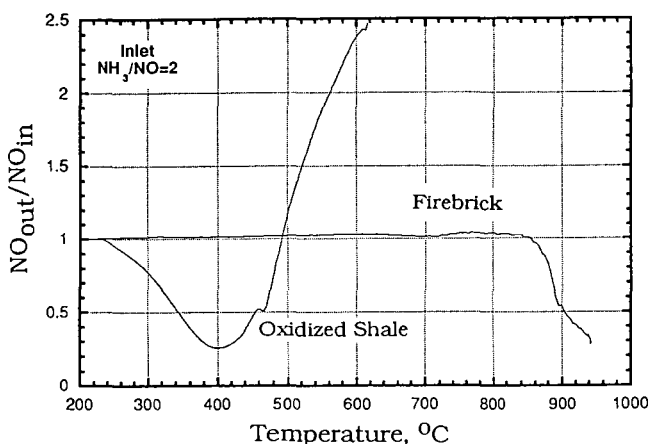
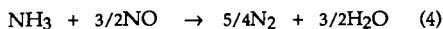


Figure 1. Loss and formation of NO from a mixture of ammonia and NO passed over heated oxidized shale and firebrick (5% O₂, NH₃/NO = 2, rate of heating 10°C/min).

NO Reduction at the Heating Rate of 10°C/min

Oxidized Oil Shale. Oxidized (combusted) Green River oil shale was heated at 10°C/min in a gas mixture of Ar with ~ 5% O₂, 2000 ppm NO, and 4000 ppm NH₃ at a gas residence time of ~ 0.6 sec from 200 to 700°C. Figure 1 shows the results. At 250°C, the NO concentration of the reactor effluent begins to decrease with respect to the NO concentration in the reactor inlet (NO_{out}/NO_{in} < 1.0). This decrease continues to 400°C where a maximum NO removal of 70% is reached. For temperatures above this maximum, NO removal activity steadily decreases. At temperatures above ~ 500°C, there is a net production of NO, which continues to increase the concentration of NO in the reactor effluent with increasing temperature.

The decrease in NO in the reactor effluent at temperatures from 250 to ~ 500°C is probably due to NO reduction by NH₃, mostly by reaction (1). Rough nitrogen balances for N₂ production and NO and NH₃ consumption support this. This behavior is in the temperature range observed for SCR of NO by commercially available V-Ti NO reduction catalysts (3). At temperatures above ~ 500°C, net NO is produced (NO_{out}/NO_{in} > 1). Rough mass balance indicates this

is probably due to ammonia oxidation, reaction (5), and nitrate decomposition (see below). Note at ~ 600°C, a large fraction of NH₃ appears to be converted to NO.

Even without NH₃ as a reducing agent, this lime-bearing sample of burnt shale (see experimental) removed NO from the gas stream at temperatures of ~ 380°C. No N₂ was released, and the amount of oxygen consumed is consistent with the following reaction for the formation of calcium or some other nitrate:



After this shale has been reacted with NO and O₂, heating above 400°C results in the release of NO and O₂, consistent with published data on the thermal stability of some nitrate compounds (7). However, x-ray diffraction did not reveal any nitrates (possibly due to low concentrations).

Firebrick. Figure 1 also shows the behavior of the same gas mixture flowing over firebrick under the same conditions. Obvious is total the lack of NO removal activity until temperatures above 850°C. This is in the temperature range assigned to thermal denox (4). Although not shown, NH₃ over firebrick (with no NO) begins to oxidize at temperatures above 500°C, not yielding any significant amount of NO, but yielding H₂O/N₂ = 3, suggesting reaction (2) is occurring. Full oxidation of NH₃ is seen only at 950°C, where thermal denox is taking place at the same time.

We presume that if the mixture of NO and NH₃ had been heated to 900°C over oxidized (combusted) shale, NO would have decreased to the values observed over firebrick. This prediction is based on the assumption that at high temperatures thermodynamic equilibrium is likely to prevail, and at 900°C, NO remains unstable with respect to N₂ and O₂.

Table 1. Removal of NO over Combusted Oil Shale (Isothermal)

Experiment, #	T, °C	NH ₃ /NO	CO ₂	NO Removal, %	~ Residence Time (sec)
1	365	2.8	No	64	0.6
2	365	0 ^a	No	19	0.6
3	375	2.8	Yes	49	0.6
4	383	2.8	Yes	50	0.6
5	374	0 ^a	Yes	8	0.6
6	385	1.3	Yes	62	1.2
7	402	1.0	Yes	63	1.2
8	385	1.0	Yes	61	1.2

a. No NH₃ in gas stream

NO Reduction at Isothermal Conditions

Figure 1 shows the temperature for maximum NO reduction over oxidized (combusted) shale is 400°C at the 10°C/min heating rate. In efforts to optimize removal conditions and obtain better mass balances, NO removal was performed isothermally over the oxidized (combusted) oil shale. Table 1 lists these results using the shale from the HRS pilot plant (contains 0.3 wt % char).

Oxidized (combusted) shale (Experiment 1). The first experiment listed in the table was carried out with the same gas composition as in the constant heating rate experiments shown in Figure 1. The NO removal is slightly lower than the maximum removal found for the constant heating rate experiment. We do not know the source of this difference, and more experiments are being performed to assess the reason. However, this may be due to the shale bed in the isothermal experiments contained little or no lime preventing NO removal by nitrate formation as a supplement to SCR.

Table 2. Normalized Nitrogen Balances for Removal of NO over Combusted Oil Shale (Isothermal)

Experiment #	<u>Consumed</u>		<u>Produced</u>	<u>Net</u>
	N from NO	N from NH ₃	N as N ₂ *	$\Sigma_{\text{pro}} - \Sigma_{\text{con}}$
1	1.00	1.46	2.58	0.12
2	1.00	0.15	2.09	0.94
3	1.00	1.44	2.44	0.00
4	1.00	1.20	2.34	0.14
5	1.00	0.10	0.11	-0.99
6	1.00	0.85	1.95	0.10
7	1.00	0.94	2.12	0.18
8	1.00	0.81	1.87	0.06

* m/z 28

Overall normalized nitrogen balance of the experiments in Table 1 are shown in Table 2. If all of the NO is consumed by reaction (1) (NO/NH₃/N₂ stoichiometry, 1/1/1; that is one N is released for each NO lost and one N is released for each NH₃ lost), an additional 0.46 moles of N from NH₃ remains to be accounted for by some other reaction. This could be almost all accounted for by the oxidation of NH₃ by reaction (2) which would produce 0.46 moles of N as N₂.

This reaction could be verified by H₂O and O₂ balances. However, O₂ and H₂O balances are complicated by the combustion of char (CH_{0.4}). For example, in experiment 1, the predicted net O₂ loss through the bed (normalized to NO as in the case of Table 2) would be 0.52 from NH₃ combustion and NO decomposition (reactions (1) and (2)) whereas the measured loss in O₂ was 2.5. The predicted H₂O production would be 2.0 but the measured production of H₂O was 2.9. The observed production of CO₂ was ~ 2, accounting for the observed extra O₂ loss. The CO₂ concentration decreased with time, due to the consumption of char. Furthermore, low temperature combustion of char can release CO (m/z 28) which may explain why more N₂ (m/z 28) was seen than can be accounted for by NH₃ and NO loss.

Oxidized (combusted) shale without NH₃ (Experiment 2). The second experiment in Table 1 shows the reaction of NO over the oxidized (combusted) shale in the absence of NH₃ as the reductant. (Very low levels of NH₃ were detected in both the inlet and product streams, probably because of desorption from prior runs, or background correction errors.) Some decrease in the NO concentration in the product effluent compared to the inlet stream does occur without the presence of NH₃. This could be through reaction (3), or by reduction by char. A 2000 ppm concentration of CO₂ is observed indicating char oxidation. A CO content of 200 ppm in the gas stream from the char oxidation chemistry would explain the observed N balance.

Oxidized (combusted) shale with CO₂ (Experiments 3 and 4). To simulate the real combustion stream for the HRS process, ~ 8% CO₂ was added to the reaction gas mixture. The third experiment in Table 1 shows the NO removal with NH₃ present in excess. Although the removal is almost 50%, which demonstrates the oxidized (combusted) oil shale has catalytic properties even with CO₂ in the gas stream, the removal is reduced to 75% of the removal found without CO₂ in the gas stream. (This is even with the reactor temperature 10°C higher.) Raising the reactor temperature from 375°C to 383°C showed only a 1% increase in removal of NO.

Table 2 shows the normalized nitrogen balance for Experiment 3. If reaction (1) is considered as the sole consumer for the NO, 0.44 moles of NH₃ reacted and 0.44 moles of N as N₂ formed remain unaccounted for. However, these remaining quantities can be accounted for by the oxidation of NH₃ by reaction (2). Although exhibiting poorer closure, the normalized nitrogen balance for Experiment 4 shows a similar result. Probably the improved N balance compared to earlier experiments is due to most of the char has been already consumed in previous experiments, so there is less contribution to m/z 28 from CO producing reactions. This is suggested because of 75% of the H₂O produced can be accounted for by NH₃ oxidation in this experiment. Also, the concentration of CO₂ in the exit gas was only 400 ppm compared to nearly 2000 ppm in the earlier experiments 1 and 2.

Oxidized (combusted) shale with CO₂ and without NH₃ (Experiment 5). The CO₂ in the gas stream also appears to have an effect on the ability of the catalyst to remove NO with or without the presence of the NH₃ reductant. Comparing the second and fifth experiments in Table 1 shows the NO removal with CO₂ but no NH₃ in the gas stream is ~ 50% lower than in the case without CO₂ in the stream. This may be due to the absence of char as a reducing agent or due to absorption (see above) instead of catalysis, suggesting the CO₂ is competing with NO for absorption sites on the shale. This will be addressed in detail in another paper.

Effect of Flow Rate and NH₃ to NO ratio on NO Removal (Experiment 6-8). Experiments 6-8 in Table 1 also show NO removal increases significantly when the gas stream residence time (containing CO₂) is doubled to ~ 1.2 sec. These conversions are comparable to the baseline case where no CO₂ is in the gas stream. Because the NH₃ to NO ratio was decreased for this set of experiments, a direct comparison to NO removal at the higher flow rate is not possible. However, these results indicate changing the flow rate (or residence time) is an important variable in maximizing the NO reaction chemistry, particularly when temperature change has an upper limit of ~ 400°C where NO formation (through reaction (5)) begins to compete.

The two experiments (6 and 8) at 385°C reactor temperature and the 1.2 sec residence time show little dependence of NO removal on the NH₃ to NO ratio. This dependence has been studied for a broader range of NH₃ to NO ratios (0 to 2.8) for thermal denox over firebrick. Those results showed a greater difference than seen for NO removal by oxidized oil shale. At 933°C, the firebrick showed for NO_{out}/NO_{in} ~ 0.48, NH₃/NO = 1.0; for NO_{out}/NO_{in} ~ 0.25, NH₃/NO = 1.30.

Table 2 shows for NH₃/NO = 1 (Experiment 8), the amount of NO reacted that can be accounted for by reduction with NH₃ (reaction (1)) is 80%. The source of the consumption of the balance of NO is uncertain. Experiment 5 at the higher gas-flow rate indicates ~ 10% decrease in NO concentration in the gas stream even when NH₃ is not present, probably by reduction by char. However, all the char was probably consumed by the time this experiment was done. Also, lime formation can not take place in the presence of CO₂ at this temperature, so NO consumption by nitrate formation probably does not occur. Reaction (3), though, when applied to

the balance of NO gives excellent N closure. Further experiments are being conducted to clarify this.

CONCLUSIONS

Oxidized (combusted) oil shale from the HRS process exhibits catalytic activity for the removal of NO from laboratory gas streams using NH₃ as the reductant. The activity and conditions have not been optimized, but typical NO removal is 60+% at a 1.2 sec gas residence time, a reactor temperature range of 380 to 400°C, and for a gas containing ~ 2000 ppm NO, 2000 ppm NH₃, and 8% CO₂. Temperature limitations potentially due to competing NH₃ oxidation suggest residence time is the important variable to study for improving removal of NO from flue gas. Optimizing this process variable, as well as application to actual retort combustor gas streams will be addressed in a later paper.

ACKNOWLEDGMENTS

We thank Russ Sanborn for assistance with the N₂O measurements, Henrik Wallman and Mary Singleton for useful discussions. This work was performed under the auspices of the U. S. Department of Energy by the Lawrence Livermore National Laboratory under contract no. W-7405-ENG-48.

REFERENCES

- 1) R. J. Cena and R. G. Mallon. 19th Oil Shale Symposium Proceedings, Colorado School of Mines, 102-125 (1986).
- 2) Clean Coal/Synfuels Letter. 4-8 Oct. 22 (1990).
- 3) H. Bosch, H. and F. Janssen. Catal. Today, 2, 369 (1988).
- 4) R. K. Lyon, Int. J. Chem. Kinetics, 8, 315 (1976).
- 5) R. W. Taylor, and C. J. Morris, Lawrence Livermore National Laboratory, UCRL-89806 October (1983).
- 6) J. B. Joshi, V. V. Mahajani, and V. A. Juvekar. Chem. Eng. Commun., 33, 1-92 (1985).
- 7) R. A. Robie, B. S. Hemingway, and J. R. Fisher. *Thermodynamic Properties of Minerals and Related Substances at 298.15 K and 1 Bar (105 Pascals) Pressure and at Higher Temperatures*, U. S. Geological Survey Bulletin 1452 (1979).